Technology Assessment and Market Analysis of Solid State Ultracapacitors

By

Zibo Jiang

B.Eng., the University of Birmingham, United Kingdom, 2006

Submitted to the Department of Materials Science and Engineering
in Partial Fulfillment of the Requirements for the Degree of

Master of Engineering in Materials Science and Engineering
at the
Massachusetts Institute of Technology

September 2007

Signature of Author.....

Department of Materials Science and Engineering

August 15, 2007

Certified by.....

Yet-Ming Chiang

Kyocera Professor of Ceramics

Thesis Supervisor

Accepted by.....

Samuel M. Allen

POSCO Professor of Physical Metallurgy

Chair, Departmental Committee on Graduate Students

TECHNOLOGY ASSESSMENT AND MARKET ANAYSIS OF SOLID STATE ULTRACAPACITORS

By
ZIBO JIANG

Submitted to the Department of Materials Science and Engineering on August 15, 2007 in partial fulfillment of the requirements for the Degree of Master of Engineering in Materials Science and Engineering

ABSTRACT

This report provides quantitative analysis of Solid State Ultracapacitors (SSUs) from technological and financial perspectives. SSUs are Ultracapacitors with solid electrolytes predicted to have huge application potential as the electrical energy storage device in Hybrid Electrical Vehicles (HEVs) due to the projected high energy density.

The potential high energy density of SSUs is achieved through engineering dielectric materials to possess high breakdown voltage and/or DC permittivity. Among the available SSU models, Electrical Energy Storage Units (EESUs) have been reported to possess energy density as high as 280 Wh/kg with the permittivity and breakdown voltage enhancements achieved through engineering composition modified barium titanate powders. Organic Solid State Ultracapacitors (OSSUs) is a proposed concept of SSUs with conductive particle filled polymer systems as the dielectric material to take advantage of the systems' giant permittivity phenomenon reported under AC. However, through experiments and modeling, such giant permittivity is not found under DC and it is thought that the reported AC giant permittivity may be strongly distorted by the eddy current loss in the commonly used equivalent circuit characterization model and therefore does not contribute to the energy density enhancement. It is also found that the geometric dispersion of conductive particles does not contribute to the energy storage capability. Hence, it is concluded that OSSU is not a competitive SSU model.

EESU would outperform current batteries in HEV applications both in terms of manufacturing cost and fuel efficiency according to the PHEV performance model. It is predicted that a typical EESU PHEV140 midsized sedan, with the estimated cost of $29,000/vehicle and the fuel efficiency of 206 mpg, would become more economically favorable than a conventional vehicle of the same size in five years based on the current energy price. The increase of the energy price will increase the relative performance of EESU PHEVs compared with battery PHEVs. Through a dynamic manufacturing model, it is predicted that the EESUs, if manufactured from 2011, would have an appreciable market share due to its superior product utility, which, in turn, transforms the product competitiveness into the corporate financial profit as soon as the sixth year of operation with 4-5 folds of return on investment in ten years.

Thesis Advisor
Yet-Ming Chiang, ScD,
Kyocera Professor of Ceramics

Acknowledgement

First and foremost, I would like to thank my parents for their unconditional support in my pursuit of higher education and career, without whom, this report would not exit.

On the academic side, I would first like to thank my thesis advisor, Professor Yet-Ming Chiang, who has shared with me his knowledge and inspiration in this promising technological field. Making such intellectual endeavor would otherwise be much less interesting without his guidance.

My gratitude also goes to my colleagues, Mr. Marco Bartosch, Dr. Ryan Wartena, Mr. Yu-Hua Kao, Miss Nonglak Meethong, Miss Miso Kim, Mr. Tim Chin and Ms. Shallow Huang in Professor Chiang's group at MIT for sharing their experience and knowledge.

My acknowledgement goes to Professor C.P. Wong and his group at Georgia Institute of Technology, who shared their experiment observation on dielectric behavior of the aluminum epoxy system.

On the industrial side, I would like to thank Mr. Ran Wang, Deputy General Manager and Chief Engineer at Aowei Technology, Inc., Shanghai, for sharing the invaluable technology and market experience of electrochemical ultracapacitors which has made Aowei Technology a successful company.

Table of Contents

Chapter 1 Introduction

We are living in a world that demands more energy than any previous periods in history. The US Department of Energy (2007) projected the global energy consumption to be doubled in the next fifty years. Along with the increasing energy consumption, the demand for low and zero emission has brought awareness to the renewable, clean and efficient energy generation and utilization. Some particular clean energy sources directly transferable into electricity, such as wind and solar energy, offer enormous potential to meet future energy needs. However, to efficiently utilize electricity generated, more efficient energy storage devices are needed. Currently, energy storage device has become a concentrated area for scientific research, public and private investments. This report will evaluate a relatively new concept of electrical energy storage device – Solid State Ultracapacitors (SSU) – in terms of technology maturity, market performance and business feasibility. The main body of the report will be divided into three chapters: Chapter 2 Technology Assessment will first layout the performance criteria for electrical energy storage device, then introduce the energy storage mechanisms in two types of SSUs – Electrical Energy Storage Units (EESUs) and Organic Solid State Ultracapacitors (OSSUs), meanwhile assessing the technology competitiveness of the two models; Chapter 3 Market Analysis will estimate of the Hybrid Electrical Vehicle (HEV) market, and then predict the performance of EESU equipped HEVs in terms of manufacturing cost and fuel efficiency; Chapter 4 Startup Manufacturing Plan will present a dynamic manufacturing plan to produce EESUs with the maximized Net Present Value from 2011 to 2020. Following the main body, Chapter 5 will survey Intellectual Properties concerning the manufacture of EESUs with comment on the related patent strategies.

Chapter 2 Technology Assessment

2.1 Performance Criteria and Types of Electrical Energy Storage Device

Two major performance criteria for any electrical energy storage device are energy density and power density. Energy density is defined as the amount of energy stored per unit mass (J/kg or Wh/kg) or per unit volume (J/L or Wh/L) of the device. Power density is a measurement of how fast energy is extracted from, or transferred into the device per unit mass (J/kg.s or W/kg) or per unit volume (W/L). The two criteria are particularly important where there is an excessive requirement for portability.

Currently, batteries and capacitors are the two major forms of electrical energy storage devices. Batteries convert chemical energy directly to electrical energy, in which charge is generated by redox reaction at electrodes and voltage is established between cell terminals depending on the chemical species and their concentrations. In Primary Batteries, this energy transformation is irreversible. In Secondary Batteries, the chemical reaction is reversible and thus the battery can be charged by supplying electrical energy to the cell. Capacitors, on the other hand, store energy by charge separation. The basic structure of a capacitor comprises of two paralleled electrodes between which a potential can be established. The dielectric electrolyte is sandwiched between the electrodes which can either be ionic liquid solution or solid dielectric material. The electrical potential can be efficiently released when a close circuit forms between electrodes, resulting in superior power density. Generally, capacitors have lower energy density due to its

inefficient materials utilization. Charges are accumulated at the thin layers of conductive electrodes and a substantial portion of the mass does not contribute to the energy storage.

Ultracapacitors are generally referred to the types of capacitors with substantially improved energy densities through various storage mechanisms. The past twenty years saw the enhancement of ultracapacitors' energy density by two decades without sacrificing too much of the power density. Known as Ragone Plot, Figure 1 positions some of the most common energy storage devices in the automotive industry on an energy density vs. power density map. The superior performance in power density and the constantly improving energy density have made ultracapacitors an attractive research and development field.

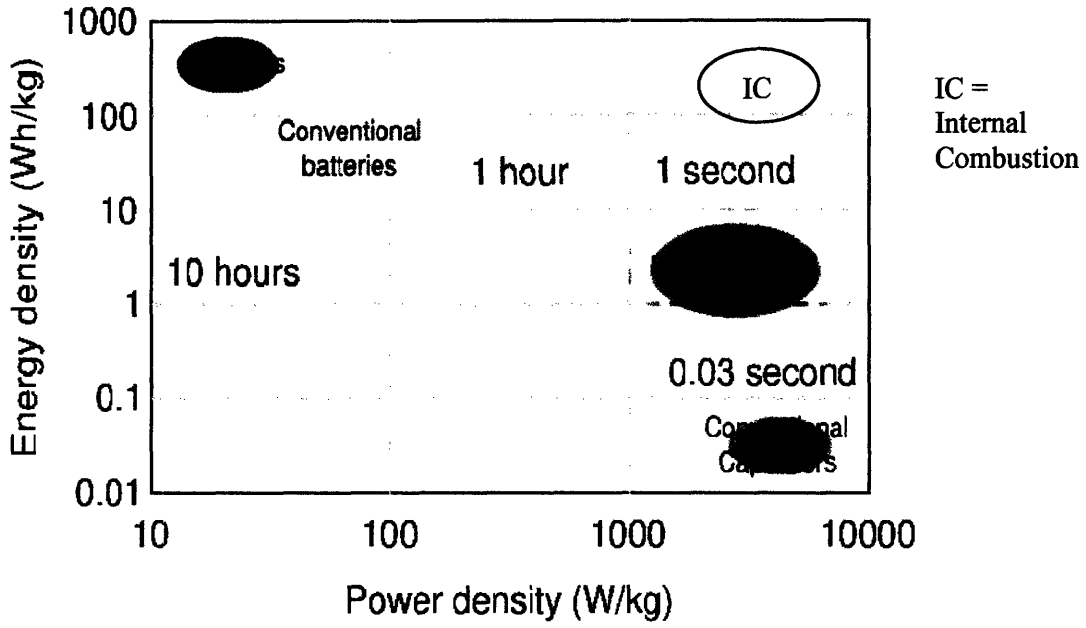

Figure 1: Ragone Plot of Power Density vs. Energy Density for Fuel Cells, Conventional Batteries, Conventional Capacitors and Ultracapacitors (Zurek 2007).

2.2 Physical Origins of Energy Storage in Ultracapacitors

In Ultracapacitors, the general form of capacitance and energy storage capability can be written by Helmholtz model (1853) in Equation 2.1 and 2.2, respectively.

$$C = \frac{A\varepsilon_0\varepsilon}{d} \qquad 2.1$$

$$E = \frac{CV^2}{2} \qquad 2.2$$

Where

C is the capacitance of an ultracapacitor (Farads),

E is the energy stored in an ultracapacitor (joules or watt hour),

ε_0 is the permittivity of free space, equaling 8.8541×10^{-12} F/m (or $C^2/(N\ m^2)$)

ε is the relative permittivity of dielectric material, or dielectric constant

A is the total surface area of electrodes (square meters)

d is space between two paralleled electrode (meters)

V is the established potential between the electrodes (volts)

From the Helmholtz model (1853), energy density per unit volume can be obtained by rearranging Equation 2.1 and 2.2 with E weighted by the device density ρ:

$$\text{Energy Density} = \frac{E}{\rho} = \frac{\varepsilon_0}{2}\left(\frac{A}{d}\right)\left(\frac{\varepsilon V_b^{\ 2}}{\rho}\right) \qquad 2.3$$

Where V_b, the breakdown voltage of the dielectric material, is used to substitute V, the operating voltage, in order to facilitate the materials property comparison among different dielectric materials

Note that Equation 2.3 consists of three parts, (1/2 ε_0) as the constant term, (A/d) as the geometry term and (ε V_b^2 / ρ) as the materials properties term. Therefore, the enhancement of energy density of ultracapacitors can be achieved through:

a) Materials property engineering by increasing dielectric permittivity ε and/or increasing dielectric breakdown voltage V_b and/or decreasing density of the dielectric materials ρ

b) Geometry engineering by increasing electrode area A and/or decreasing electrode distance d

Different models of ultracapacitors concentrate on the manipulation of one or several parameters in categories a) and/or b). The next section will introduce different ways to improve energy density in different types of ultracapacitors.

2.3 Electrochemical Capacitors (ECs)

Electrochemical Capacitors (EC) or Double Layer Capacitors (DLC) are the most maturely developed ultracapacitors[1] and thus are considered conventional ultracapacitors. Invented in 1957 by H. I. Becker of General Electric (U.S. Patent 2,800,616), the structure of EC requires two electrodes immersed in ionic solution, where charge is accumulated at the double layer interface. Currently, they are mostly used as the energy storage device in regenerative breaking systems in Hybrid Electrical Vehicles (HEVs) and intermittent energy generation systems such as solar and wind power facilities. As Figure 2 shows, compared with traditional capacitors with solid electrolytes, the improvement of energy density of EC comes from the lighter ionic solution (smaller ρ).

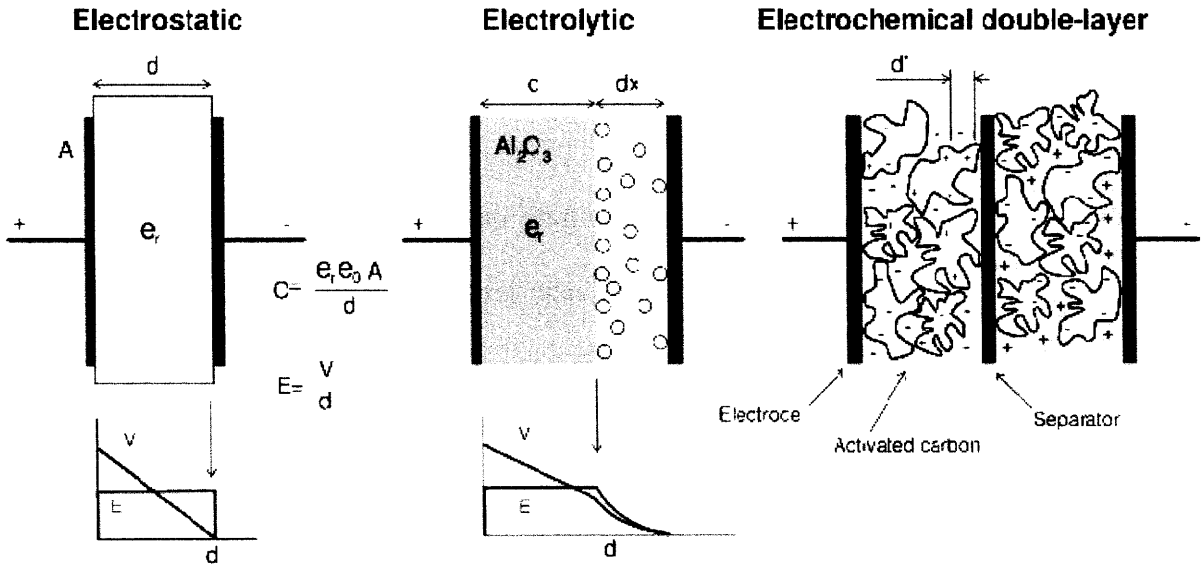

Figure 2: Structural comparison among electrostatic capacitors, electrolytic capacitors and electrochemical capacitors (ECs) (Zurek 2006)

[1] ECs were first commercialized in 1978 by NEC in its electric power switching device under the trademark of SuperCapacitorTM (NEC 2007).

New generations of ECs provide the following mechanisms in the continuous improvement of energy density:

a) Enhancement of active material permittivity ε

The use of carbonaceous active material as the electrode current collector was introduced by US Nanocorp, Inc. in US Patent 7,199,997 (06/09/2000), which acts to increase the permittivity and reduce the weight.

b) Enhancement of electrode area, A

Nanostructured materials possess high accessible surface area A, leading to high capacitance and high energy density. Table 1 shows the energy storage performance of EC with carbon based nanostructured electrodes. Recent research by Signorelli (2002) utilized vertically aligned carbon nanotubes (CNT) as electrode material. This unique CNT forest structure (Figure 3) possesses extremely high electrode surface area up to $2000m^2/g$. A resultant energy density of 60 Wh/kg was reported, comparable to that of lithium ion batteries (120 Wh/kg).

Table 1: Capacitance and Energy Density of Positive Electrode Materials Discussed in US Patent 7,199,997

Example	Type of Carbon	Wet mass of Carbon (mg)	Type of MnO_2	Wet mass of MnO_2 (mg)	Capacitance (F)	Energy (J)	Wh/kg
1	particulate	100	particulate	165	5.1	7.4	7.7
2	particulate	100	particulate	125	3.9	5.7	7.0
3	particulate	100	nanostructured	175	5.4	7.8	7.9
4	nanofibrous	800	particulate	165	6.3	9.2	2.6
5	nanofibrous	800	nanostructured	210	7.5	10.8	3.0

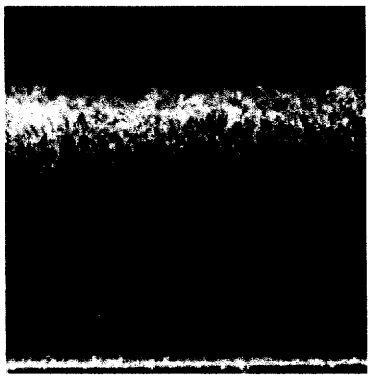

Figure 3: TEM image of CNT forest grown on aluminum electrode, which provides straight pathways so the ions could be conducted more efficiently and packed more neatly. Each nanotube is about 250 micrometers long (Baughman et al 2002).

Asymmetric ECs[2] is a new concept of ECs with further improved energy density by engineering one of the electrodes to have lower degree of polarization, P. The following mechanisms are brought forward by this feature:

c) Larger operational voltage during charge and discharge

The established electric field across the electrodes, E, and the polarization, P, bear the following relationship:

$$E = \frac{P}{\chi \varepsilon_0} \qquad 2.4$$

Where χ is electric susceptibility, ε_0 is permittivity of free space. The difference in polarizability of two electrodes helps to develop a large window of potential during charge and discharge, shown in Figure 4. The resultant higher voltage provides almost a four-fold increase in energy density.

[2] Asymmetric ECs were introduced in US Patent 5,986,876 by Stepanov et. al (11/16/1999). They are used as the major energy storage device in Shanghai Urban Bus Route 11, the first commercialized all-ultracapacitor power system in public transportation (Aowei 2007)

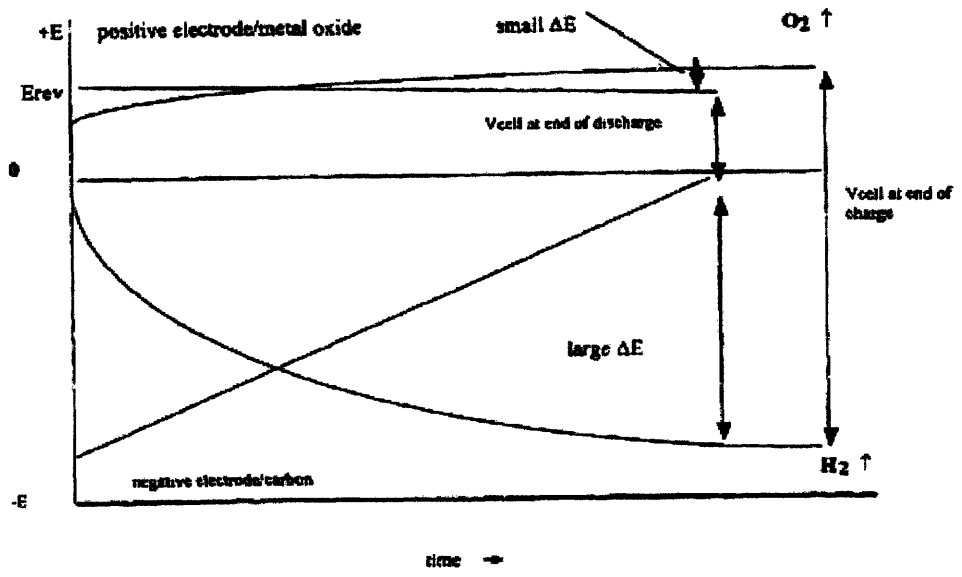

Figure 4: Illustration of enlarged charging and discharging potential window as a result of asymmetric electrochemical ultracapacitor (Lipka et. al US Patent 7,199,997)

d) Increased overall capacitance

Different polarizabilities of two electrodes lead to different electrode capacitances. The overall capacitance, C, has the following relationship with that of the two individual electrodes:

$$\frac{1}{C} = \frac{1}{C_1} + \frac{1}{C_2} \qquad 2.5$$

Thus, the overall device capacitance is increased due to the asymmetric factor, leading to higher energy density.

e) Increase mass efficiency

Because one electrode material has such high capacity, its mass can be substantially reduced, thereby increasing the device energy density.

2.4 Introduction to Solid State Ultracapacitors (SSUs)

Solid State Ultracapacitors (SSUs) are a new concept of Ultracapacitors with solid electrolyte materials. During the last decade, industries and researchers have started to become interested in SSUs due to the potentially higher breakdown voltage of solid electrolyte, ease of manufacture and higher degree of portability. Therefore, they can potentially find wider market acceptance in automotive industry and other industries with stringent requirements for energy density and portability. EEStor Inc., a Texas based startup company, has been trying to commercialize ceramic electrolyte based ultracapacitors, called Electrical Energy Storage Units (EESUs), based on series of US Patents received by EEStor's ECO, Richard Weir. Another SSU model is also proposed to utilize conductive polymer filled composite as the electrolyte material and thus named Organic Solid State Ultracapacitors (OSSUs) by the author. Based on several literatures, such composite systems have demonstrated giant permittivity phenomenon operating under AC (Isomil 2006 and Moya 2000). If such giant permittivity also exists under DC, the energy density of OSSUs can be manipulated to increase exponentially.

2.4.1 Solid Electrolyte Materials Selection Criteria

Although the energy storage mechanisms of EESUs and OSSUs differ from each other, the innovations commonly concentrate in the engineering of the solid electrolyte materials. Furthermore, the materials selection criteria for the electrolyte are similar since

both models are originated from the electrostatic capacitors[3]. Based on the established energy density function in Equation 2.3, we can single out the materials property term and the general materials selection criterion for the electrolyte materials expressed in Criterion i):

i) $(\frac{\varepsilon V_b^2}{\rho})$ is maximized

Hence, through the careful selection and engineering of dielectric materials, effort shall be made to increase both the permittivity ε and dielectric breakdown strength V_b while minimizing density ρ. Due to the square factor on V_b, priority should be given to the enhancement of electrolyte breakdown strength in the multi-parameter manipulation.

2.4.2 Direct Current (DC) Operation

Direct current operation is a common operating parameter for both EESUs and OSSUs to enhance energy storage through the maximization of dielectric medium permittivity[4] which strongly depends on the electric field frequency. Shown in Figure 5, the real part of permittivity, relating to how much charge can be stored in a given electric field, decreases with increasing frequency as more dipole mechanisms act to dissipate energy. Therefore, Direct Current (DC) operation maximizes dielectric permittivity by avoiding energy dissipation at higher electrical field frequencies.

[3] The basic structure of electrostatic capacitor comprises of block of dielectric material sandwiched by paralleled conductive plates shown in Figure 2.

[4] Permittivity describes how an electric field affects and is affected by a dielectric medium and is determined by the ability of a material to polarize in response to an applied electric field (Bottcher 2001).

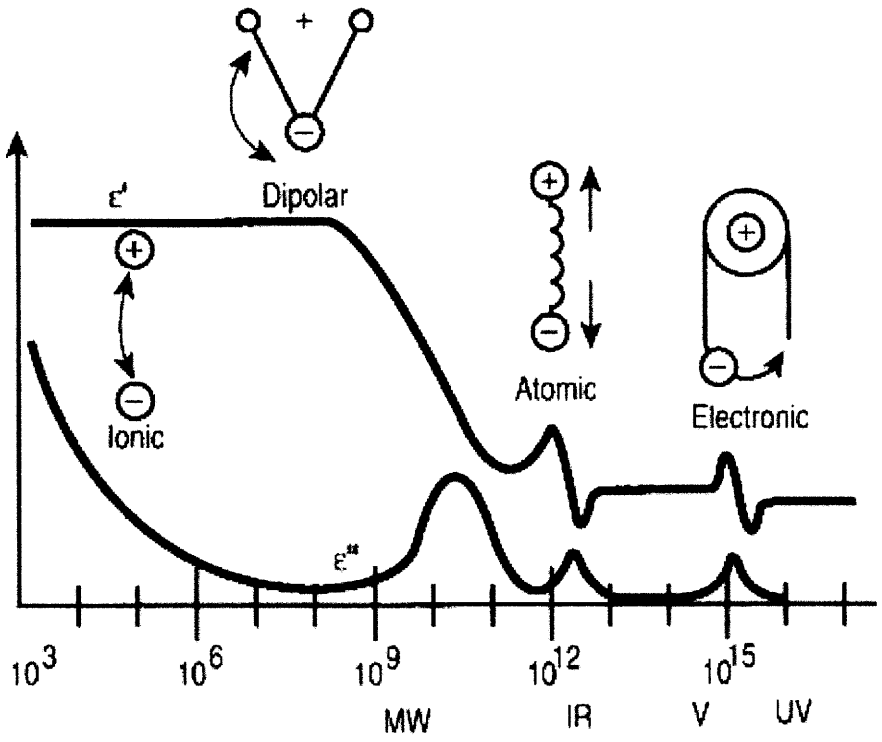

Figure 5: Real and imaginary parts of dielectric permittivity versus frequency with several dipole mechanisms (ionic, dipolar, atomic and electronic) labeled (Search.com 2007)

2.5 Electrical Energy Storage Unit (EESU)

The concept of an ultracapacitor based on the solid electrolyte with high permittivity and breakdown voltage was introduced in US Patent 6,078,494 by Hansen in 1998. The concept was further developed in series of patents by Weir et al. (see Section 5.1) who named such device Electrical Energy Storage Unit (EESU). Based on these intellectual properties, EEStor Inc., a Texas based startup company, aims to produce EESUs as the major energy storage device for Electrical Vehicles (EVs). EEStor has signed a contract to commercialize EESU equipped vehicles with Feel Good Car Company and planned to make the first generation ZENN Electrical Vehicles roadworthy in 2008 (ZENN 2007).

2.5.1 Choice of Materials

The dielectric electrolyte of EESU comprises of the basic material of a high permittivity composition-modified barium titanate (barium-calcium-zirconium-titanate) ceramic with suggested modified ceramic phase of alumina and glass phase of calcium magnesium aluminosilicate.

Due to its perovskites noncentrosymmetric crystallographic structure, barium titanate is a ferroelectric material and easily dipolable in response to the applied field and thus possesses high susceptibility, χ, which bears the following relationship with permittivity:

$$\varepsilon = (\chi + 1)\varepsilon_0 \qquad 2.6$$

As a result, pure barium titanate possesses extremely high permittivity in the order of 10^3 and 10^4. However, high permittivity dielectric materials have some inherent issues including ageing, fatigue and dielectric property degradation. US Patent 07,033,406 (2006) provides the solution by sealing barium titanate powders with double layers of alumina (Al_2O_3) and calcium magnesium aluminosilicate ($CaO.MgO.Al_2O_3.SiO_2$) to eliminate base particles' inherent problems. In addition, the two modification phases possess superior dielectric breakdown voltages as high as 5.10^6 V/cm (Kuwata et al. 1985), substantially increasing the potential energy density.

2.5.2 Microstructure Engineering

The purpose of microstructure engineering of dielectric ceramics is to further enhance dielectric breakdown strength, eliminate electrical leakage and enhance manufacturability. In the dielectric materials, any voids or porosities tend to concentrate electrical field and deteriorate breakdown strength of the electrolyte. The high tendency to form porosity in ceramic systems poses a significant challenge as to eliminate porosities.

One solution is the formation of bi-layered coatings of aluminum oxide and calcium magnesium aluminosilicate glass around the calcined barium titanate powder upon heating the nominal powder composition. These coating structure provides two mechanisms in the enhancement of dielectric breakdown strength: first, the coating materials' inherent high breakdown strength increases the breakdown strength of base particles to 3.10^6 V/cm; second, the glass coating becomes easily deformable at 800°C, which assists removing the voids from the dielectric component when elevated temperature and pressure is applied. In addition, the glass coating effectively lowers the sintering temperatures, allowing nickel to be used as electrode material instead of platinum or gold, providing a major cost saving (Weir et al. 2001).

2.5.3 EESU Structure and Manufacture Method

The basic EESU component is interleaved multilayers of alternating nickel electrode layers and double-coated composition modified barium titanate as illustrated in sub-

figure 2 of Figure 6. Individual unit of capacitors are then put in parallel and stacked on one another to the desired capacity as illustrated in sub-figure 3 and 4 in Figure 6.

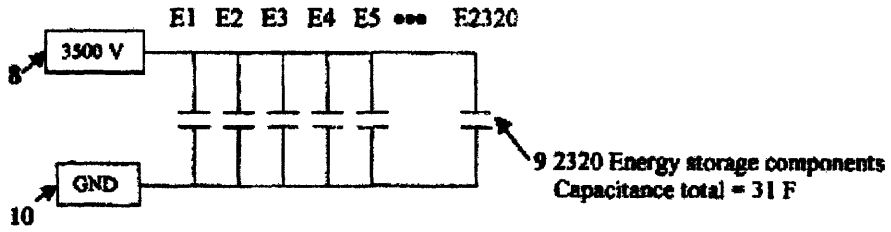

Figure 1

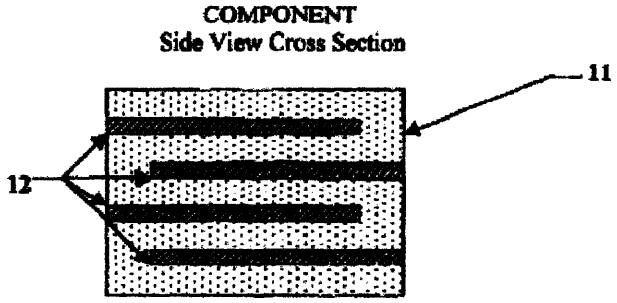

Figure 2

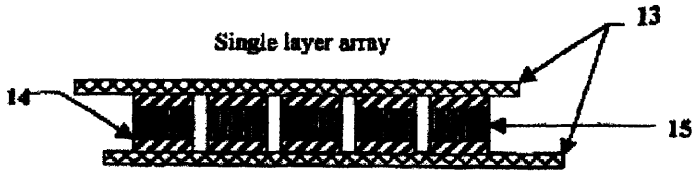

Figure 3

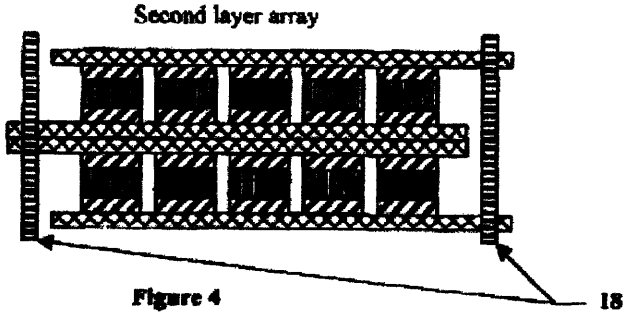

Figure 4

Figure 6: EESU Structure, (1) abstract capacitor equivalent, (2) side view cross-section of multilayered array, (3) single layer array of capacitor in parallel, (4) two layer array of EESU stack (US Patent 6,078,494)

Figure 7 demonstrated the basic process flow of producing EESUs stacks of desired capacity. Starting with wet-chemical processed and calcined barium titanate powders, ceramic layers and glass layers are coated onto the basic powders by wet chemical process. The coated powders are then screen printed with nickel powders to form an alternating layered structure, followed by sintering to a closed-pore porous body. Hot-Isostatic Pressing (HIP) then applies elevated pressure and temperature to the sintered body to form a void free component. The optimal heat treatment schedule is illustrated in Figure 8. At the packaging stage, the paralleled components are connected with nickel bars and configured with the use of a solder-bump technique. Section 5.1 details the process and conditions according to US Patent 6,078,494.

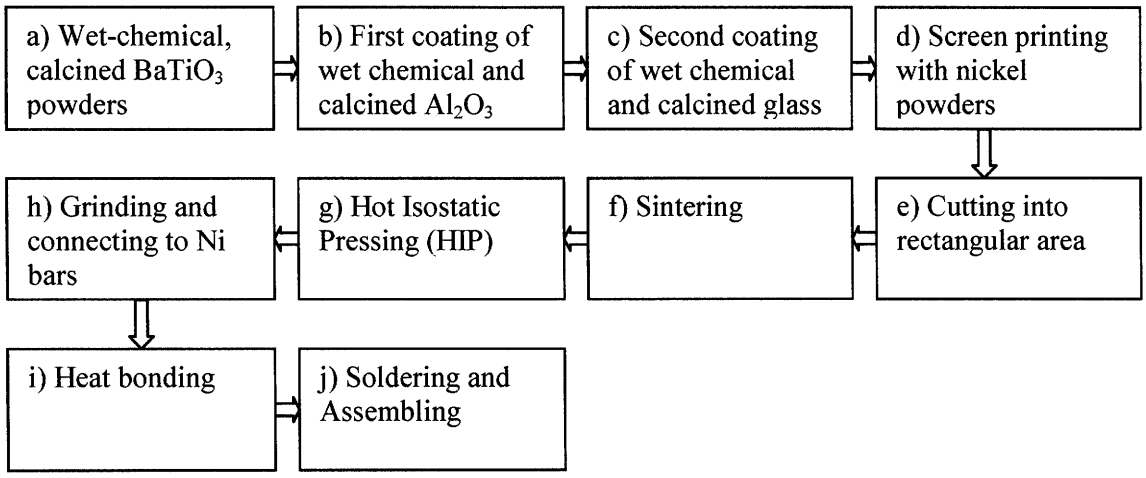

Figure 7: Basic process flow sheet of producing stacks of EESUs, based on US Patent 6,078,494

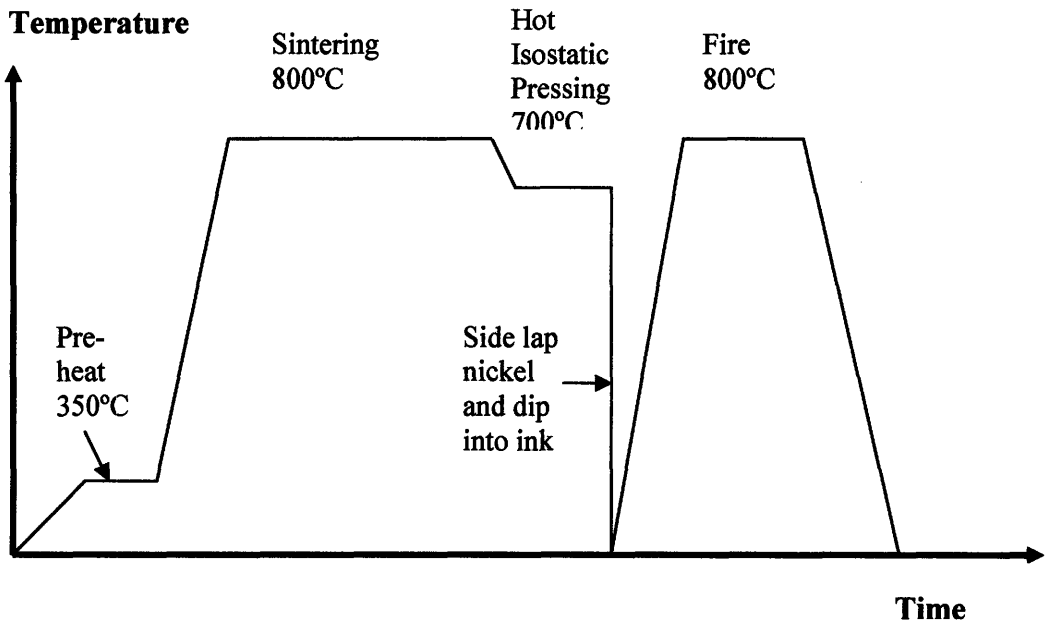

Figure 8: Heat treatment schedule for a single layer of ceramic dielectric and nickel electrode in EESU (from Process f to g in Figure 7 (a))

2.5.4 Predicted Performance of EESU

Based on the theoretical estimation, Weir et al. (2001) predicted that the superior performance of EESU could potentially revolutionize the Electric Vehicle (EV) industry.

Through the initial experiments, energy density as high as 280 Wh/Kg was reported, twice that of the lithium ion batteries, quadrupled that of the best electrochemical capacitors (EC) and ten times that of lead acid battery. A high power density of 100 kW/kg was also reported, making EESU extremely efficient to charge and discharge. The predicted advantage of EESU also include extremely long life cycle of about 1,000,000, superior to most available ECs and batteries.

The unit manufacturing cost of EESU was reported to be one-eighth of the manufacturing cost of an equivalent lithium ion battery in most portable computer and mobile gadgets today (Terjepetersen 2007). This estimation, however, is questionable mainly due to the high materials cost as laid out in Chapter 4. The ceramic solid-state electrolyte would have less severe overheating compared to chemical battery, reducing some safety concerns; the lack of hazardous materials in its electrolyte composition would make EESU potentially a clean energy storage device. Weir et al. (2001) made a performance comparison among different types of batteries and the predicted performance of EESU shown in Table 2.

Table 2: Comparisons of Major Performance Parameters among Different Types of Battery and Ceramic EESU

The parameters of each technology to store 52.2 kW · h of electrical energy are indicated-(data as of February 2001 from manufacturers' specification sheets).

	NiMH	LA(Gel)	Ceramic EESU	Ni—Z
Weight (pounds)	1716	3646	336	1920
Volume ($inch^3$)	17,881	43,045	2005	34,780
Discharge rate	5%/30 days	1%/30 days	0.1%/30 days	1%/30 days
Charging time (full)	1.5 hr	8.0 hr	3–6 min	1.5 hr
Life reduced with deep cycle use	moderate	high	none	moderate
Hazardous materials	YES	YES	NONE	YES

To help the readers to visualize an EESU equipped vehicle according to the above performance data, we can logically assume an EESU device to power a 40 hp sedan running at 60 mph for 5 hours before the next recharge. Such an EESU needs to have at least 2320 individual capacitors in parallel operating at a voltage of 3500 V, occupying a total space of 2005 $inch^3$, weighing 336 lbs, three times the battery weight of a Toyota Prius NHW11 (Toyota 2007).

2.5.5 Technology Uncertainties

Some technology challenges may hinder EESU in achieving the claimed performance in automotive industry, among which the biggest concerns include leakage current, mechanical integrity and the safety issue. Extremely high operating voltage in an electrostatic capacitor may result in high leakage current (Miller 2007), significantly deteriorating the energy pertaining time. As always an issue for ceramic components, brittleness has been considered as an intrinsic source of failure for EESU's operation under low temperatures. Current internal combustion systems are required to operate as low as -40 °C. In the last performance review, however, EEStor (2007) has increased the lower boundary of EESU's operating temperature from -40 °C to -20 °C, suggesting the brittle nature of EESU remained an issue. Safety is another issue when a 3,500-volt-charged EESU moving at high speed. Weir (2007) defended that the voltage will be stepped down with a bi-directional converter and the whole system will be secured in a grounded metal box. Other issues that may increase the technology uncertainties include quality control, operating reliability and device over-heating.

2.6 Organic Solid State Ultracapacitors (OSSUs)

Organic Solid State Ultracapacitors (OSSUs) is another type of Solid State Ultracapacitors (SSUs) based on the model of electrostatic capacitors. The proposed dielectric material is conductive particles filled polymer composite with the basic materials selection criterion satisfies Criterion i) under DC operation described in Section 2.4.1.

2.6.1 The Discovery of Giant Permittivity

In initial proposal of making a SSU from the conductor-insulator system was raised by Pecharroman and Moya (2000) in wake of their discovery of the giant capacitance phenomenon at the neighborhood of percolation threshold[5] in Mo/mullite system. They found at frequency as high as 10 MHz, the system permittivity ε following an empirical scale law with the conductive particle loading level, f, below percolation threshold, f_c:

$$\varepsilon = \varepsilon_D (f_c - f)^{-s} \qquad f < f_c \qquad 2.7$$

Where

ε_D is the permittivity of polymer matrix

s is the characterizing exponent in a fixed system dimensionality, e.g., s = 0.7 for a three dimensional system.

[5] In conductive insulating composite systems, the particle connectivity allows the electrical conductivity of the system to change discretely from being insulating to conductive. This sudden change in electrical conductivity occurs when the loading level of conductive particle increases to a critical value, f_c, which is defined as the percolation threshold

Such giant permittivity phenomenon was demonstrated in Pecharroman and Moya (2000)'s experiment shown in Figure 9. The scaling relationship of permittivity and conductive particle loading near the percolation threshold was found in some other systems. Figure 10 shows the trend of system permittivity in carbon black particle filled polyethylene system measured at a frequency of 10 kHz (Isomil, 2006).

Isomil (2006) attributed the physical origin of the giant permittivity to be that electric charges accumulate at the conductor insulator interface and that the development of this interfacial charge polarization within the bulk material contributes to huge dielectric constants. As the concentration of these conducting centers increases near the percolation threshold, the large numbers of conductive regions, each separated by very thin insulating barriers lead to huge bulk permittivity. Thus giant permittivity phenomenon can occur at the neighborhood of the physical percolation threshold.

If this phenomenon holds true in conductive/insulating composite systems under the DC operation, a Solid State Capacitors (SSUs) with such material system as the dielectric material can take advantage of the giant permittivity phenomenon near the percolation threshold and therefore possess greatly enhanced energy density. Up to date, no literatures have reported the successful production of such SSUs. Hence, it is of value to assess the technology feasibility of such proposal through experimental and modeling approaches.

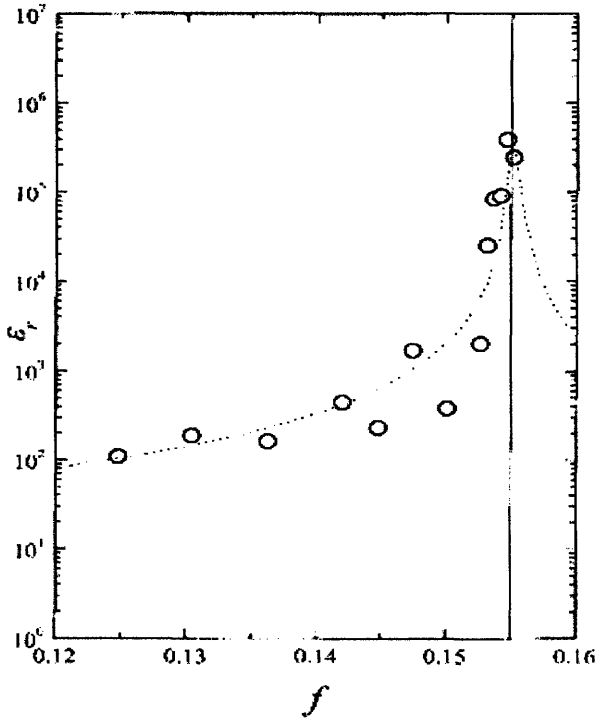

Figure 9: Permittivity of Mo/mullite system versus Mo concentration, measured by a two-point technique at 10 MHz and curve fitted to Equation 2.7. Vertical line indicates the percolation threshold (Pecharroman and Moya 2000).

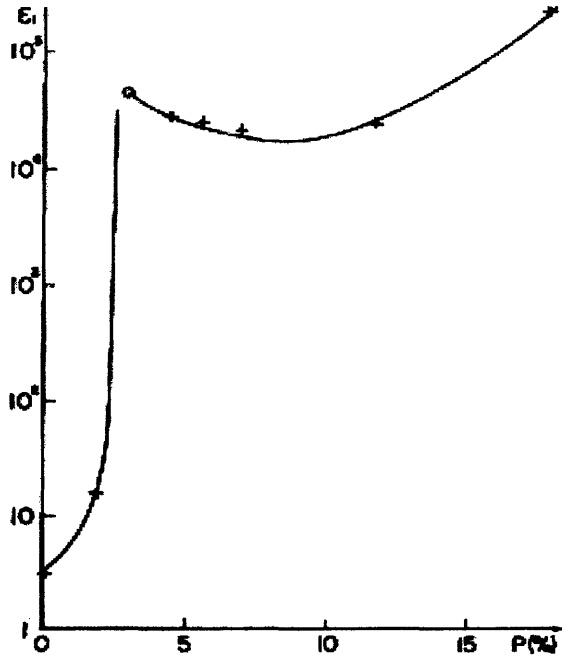

Figure 10: Carbon black C1 loading level p vs permittivity of carbon/polyethylene composite at AC (10 kHz) (Isomil 2006).

2.6.2 Dielectric Breakdown Strength Assessment

Dielectric breakdown voltage is another important factor contributing to the energy density of the potential OSSUs. Intrinsic breakdown voltage depends on the number of mobile electrons in the insulator and upon their energy distribution. Generally, a polymer system with inherent high dielectric breakdown voltage would provide a high background breakdown voltage for the composite system. The polymer systems listed in Table 3 are the potential candidates for the matrix material.

When the polymer matrix is blended with conductive particles, several factors can adversely affect the breakdown voltage of the polymer composite:

1) **Conductive Particle Loading Level and Porosities**

The increase of conductive particle loading level or the amount of porosities deteriorates the system breakdown voltage (Isomil 2006). This is because both conductive particles and porosities in the composite system will concentrate electric field, resulting in localized electrical field being much higher than what is actually applied.

2) **Agglomerated particle size distribution**

Isomil (2006) also suggests that the wider size distribution of agglomerated conductive particles lowers the dielectric strength.

Externally, some chemical modification in matrix polymers can help disperse the conductive particles (Isomil 2006) and hence facilitate the achievement of higher breakdown voltage.

To conclude, in the assessment of the OSSU concept, the answers to the following questions will critically determine its technology feasibility:

i) Whether the giant permittivity phenomenon exist under DC operation

ii) Whether the dispersion of conductive particles in the composite system contribute to the energy storage capacity

iii) Whether the system breakdown voltage support the enhancement of energy density

Table 3: Dielectric Properties of Selective Polymers with Relatively High Breakdown Strength

Material	Breakdown Strength (V/cm)	Dielectric constant
Polyethylene (HDPE, Molded)	20000	2.3
Polyethylene (LDPE, Molded)	19000	2.3-2.6
Polypropylene, Molded	22000 - 140000	2.2 - 2.3
Polyphenylene Sulfide (PPS); Molded	11000 - 24000	3 - 3.3
Polyimide	22000 - 27600	3.4 - 3.55
Polystyrene	42910 - 64000	2-2.28
PVDF (Arkema Kynar® FLEX 2801)	**10000-27000**	**6.8**
Polycarbonate (Extruded)	30000	2.9
Polybutylene (PBT, Extruded)	26000	2.88-3.2
Polyethylene Terephthalate (PET, Unreinforced)	18000	3
Polyester (Rigid, thermoset)	14000-18000	5.5
Polyether	27000	4.7
PVC, Extruded	18000 - 18600	3.3
Polyether Block Amide (PEBA)	5000 - 44500	>3
Polyester Thermoplastic Elastomer	19700	4.6 - 4.9
Polyphenylsulfone (PAS)	14200 - 20000	3.4 - 3.5
Silicone Elastomer	16000 - 26000	2.15 - 5.4
Polyarylate	18000	3.1
Polyarylamide	34000	2.8
Nylon 66, Unreinforced	17000 - 120000	3 - 5
Nylon 6, Unreinforced	14000 - 100000	3 - 7
Polytetrafluoroethylene (PTFE), Extruded	24000	2.1
Epoxy, Cast, Unreinforced	**16000**	**4**
Acrylic, Extruded	15000 - 60000	2.8 - 3.2
Acetal Copolymer, Unreinforced	16500 - 85000	3.7 Min
Acrylonitrile Butadiene Styrene (ABS), Molded	15700 - 34000	2.7 - 3.2

Source: Matweb 2007

The bolded materials were used as the polymer matrix in the experiments detailed in Section 2.7

2.7 Experiments

2.7.1 Objective and Requirement

This section will present the experiments conducted in the effort to produce the electrolyte for Organic Solid State Ultracapacitors (OSSUs). The main objective of the experiments is to find a material system possessing competitive or superior energy density compared to the current battery systems. To conclude from the conceptual dielectric material system discussed in Section 2.6, the ideal requirements for such system include:

- Operation under direct current (DC)
- Polymer matrix with high breakdown strength
- Narrowly distributed conductive particles well dispersed in the polymer matrix
- Elimination of void or porosities
- Composite system with a low percolation threshold
- Having the conductive particle loading level just below the percolation threshold
- The use of chemical modification if necessary

2.7.2 Materials and Sample Preparation

Two conductive particle filled polymer systems were produced and characterized to meet the above requirements:

1) Aluminum powders dispersed in Polyvinylidene Difluoride (PVDF) solution
2) Aluminum powders dispersed in epoxy resin

Aluminum powders were chosen because of the conducting characteristics and cost effectiveness. The powders were provided by Alfa Aesar with the specification summarized in Table 4. Particles of different sizes were chosen as one variable to identify the size effect on the energy storage capability.

Table 4: Specifications of aluminum powders

Al powders (UN 1396)	Average Diameter (μm)	Oxide Layer Thickness (nm)	Tap Density (g/cc)	Morphology
Alfa Aesar 43891	0.1	N/A	0.3	Spherical
Alfa Aesar 41000	3.0 – 4.5	2.5 - 3	1.5	Spherical
Alfa Aesar 11067 Mesh -325	7 - 15	N/A	1.9	Spherical

For the polymer matrix, both PVDF and epoxy resin possess relatively low density and high breakdown voltage shown in Table 3.

Aluminum/PVDF System

As a ferroelectric thermoplastic polymer, PVDF possesses relatively high intrinsic permittivity[6]. The PVDF used in this experiment is Kynar 2801 with a permittivity of 6.8, breakdown voltage of 760,000 V/cm and density of 1.78 g/cc (Matweb 2007). As a thermoplastic, PVDF needs to be dissolved in acetone solution in order to facilitate the well dispersion of aluminum particles and the establishment of cross-linking after dried. PVDF also possesses relatively low dissipation factors and good thermal and chemical stability.

The samples were made in the following sequence: in argon atmosphere, aluminum powders, PVDF powders and acetone were weighed and mixed with the desired composition by a balance to the sixth decimal accuracy. The solutions were manually homogenized in a flat-bottom glass bottle before transferring to an ultrasonic shaker operating for an hour. After the ultrasonic shaking, the solutions were again manually shook and then left dried in 1) argon and room temperature atmosphere for 24 hours; 2) air and 100°C drying oven for 24 hours. As a result, cylindrical samples were obtained which could be cut into desired size to fit into characterization tools (e.g. Swagelok Cells).

Aluminum/Epoxy Resin System

As a thermoset, epoxy resin was first mixed with aluminum particles weighed to the desired composition by a balance to the sixth decimal accuracy. The solutions were well homogenized by mechanically stirring and ultrasonic shaking. Epoxy resin hardener was

[6] The backbone of PVDF, $-(CH_2CF_2)_n-$, possessing high polarizability, determines the high value of permittivity.

then mixed with the solution with the weight ratio to the applied epoxy of 1:1. The final solutions were then sandwiched between two paralleled Cu foil (Alfa Aesar 100 μm thickness) substrates illustrated in Figure 11 (a) and (b). After dried in air under room temperature for 24 hours, Cu sandwiched composites were cut into the desired size. Aluminum particle loading levels from 0 vol% to 70 vol% were produced, with 5 vol% of intervals from 0 vol% to 20 vol% and 10 vol% of intervals from 20 vol% to 70 vol%.

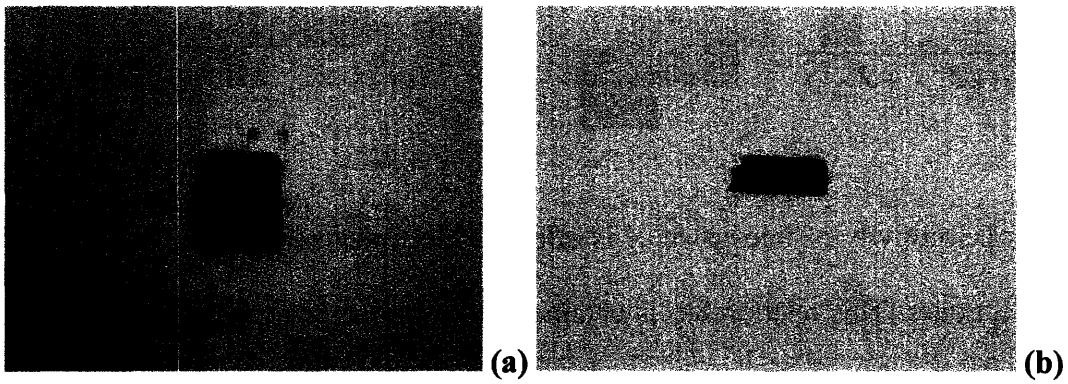

Figure 11: Sandwich structure of Al/Epoxy resin samples with Cu foil as electrodes and Al/Epoxy resin composite as electrolyte (a) Plan view (b) Side view

2.7.3 Materials Characterization

The sample density was characterized by water emersion method (Archimedes Method). By comparing the characterized density with that of the ideal mixed density (assuming dense body), the degree of porosity level can be calculated.

The permittivity was calculated from the impedance measurements by a Solartron SI 1287 Impedance Spectroscope from which three sets of correlations were directly obtained: 1) real part of impedance Z_{Re} versus imaginary part of impedance Z_{Im}, 2) Z_{Re} versus applied frequency ω and 3) Z_{Im} versus ω. The relationship between the system permittivity and the components of impedance is presented by Marsoukov and Macdonald (2005):

$$\varepsilon = \frac{-Z_{\mathrm{Im}}}{(\varepsilon_0 \omega A/t)(Z_{\mathrm{Re}}{}^2 + Z_{\mathrm{Im}}{}^2)} \qquad 2.8$$

Where ε_0 is permittivity of free space, A is effective electrode area and t is the distance between electrodes. This relationship is obtained based on the equivalent circuit model[7] which deals with the variation of total impedance in the complex plane (Bard and Faulkner 2001). For all impedance measurements, the amplitude of the applied voltage is 1000 mV; the frequency range was set to be between 0.1 Hertz and 10^6 Hertz. The permittivity calculation in this report will be based on Equation 2.8. For each data point, two samples were characterized and the average was used in bulk property analysis. Up to date, the characterization of breakdown voltage has not been conducted.

[7] Equivalent Circuit Model is based on the assumption that the performance of an electrochemical cell can be represented by an equivalent circuit of resistors and capacitors that pass current with the same amplitude and phase angle that the real cell does under a given excitation (Bard and Faulkner 2001).

2.8 Results and Discussion

2.8.1 Aluminum/PVDF System

A typical volume distribution of aluminum powder (0.1 μm), PVDF polymer and porosity is shown in Table 5. Although generally, the porosity level decreases with the increase of aluminum particle size due to the higher tap density and less inter-particle space, the porosity volume invariably contributes to more than 50% of the bulk volume. The reason for this excessive porosity level is thought to be that 1) high volatility of acetone solution during the sample drying resulted in insufficient time for the PVDF chains and aluminum particles to intermingle and eliminate porosities among them; 2) relatively high Al/PVDF solution viscosity resulted in the porosities being trapped in the solution.

Such high porosity levels are extremely detrimental to the achievement of high breakdown voltage. Although some process improvements have been conducted to systematically eliminate porosities, such as operating under reduced pressure to increase pressure gradient or elevated temperature to reduce viscosity, it has so far been observed that porosity volume percentages remained in the detrimental regions.

Table 5: Bulk sample volume distribution of aluminum powder (0.1 μm), PVDF dried polymer and porosity

	Mass (g)	Density (g/ml)	**Volume**	**% Vol**
Al 0.1 μm	1.29	2.7	**478**	**12.3**
PVDF	0.652	1.77	**368**	**9.5**
Porosity	0	0	**3047**	**78.2**
Total	1.942	0.4988	**3893**	**100**

2.8.2 Aluminum/Epoxy resin System

The near void-free samples were obtained for the Al/Epoxy resin system. Figure 12 (a) and (b) are optical microscope X50 images of 5 vol% and 30 vol% of -325 Mesh Al (17 μm) dispersed in epoxy resin matrix, respectively. It is shown that the particle agglomeration becomes significant when the loading level increases, which would have a negative effect on the system breakdown voltage.

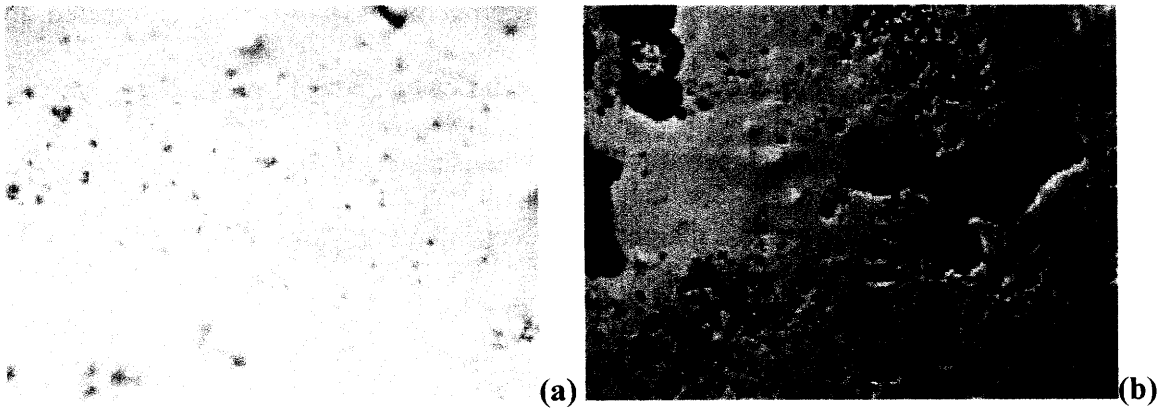

Figure 12: Optical microscope image (X50) of -325 Mesh Al/Epoxy Resin (a) 5 vol% Al loading, (b) 30 vol% Al loading

2.8.2.1 Absence of Electrical Percolation

Samples of all loading levels (0 vol% to 70 vol%) show the electrical resistivity higher than 10^6 ohms.cm, indicating the absence of electrical percolation. Such absence was also reported from Wong (2007)'s experiments on a similar Al/Epoxy system, which may be attributed to the formation of self-passivation layer around Al particles, insulating the physically percolated particles.

2.8.2.2 Absence of Giant Permittivity Phenomenon under DC

Figure 13 shows the relationship between the average permittivity in -325 Mesh Al/Epoxy Resin at different loading levels under DC field. The overall DC permittivity ranges from 20 to 60 for the Al loading levels from 5 vol% to 70 vol%. Permittivity peaks at the loading level of 10 vol% and experiences a dramatic increase at loading levels higher than 50 vol%. Although the giant permittivity could appear near the physical percolation threshold in the absence of electrical percolation (Valant et al. 2006), this phenomenon, characterized by the scale-law increase of the system permittivity, is not apparent in Al/Epoxy resin system operating under DC.

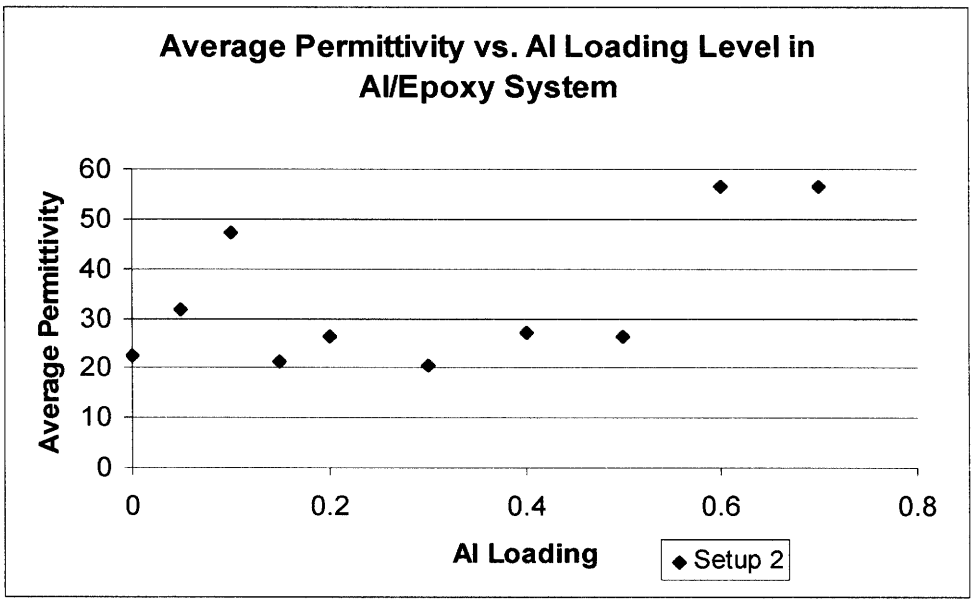

Figure 13: Average permittivity vs. Al loading level in -325 Mesh Al/Epoxy system

To generalize the relationship between permittivity and particle loading level in the system of conductive particle filled insulating composite, Carter (2007) at Masacchusetts Institute of Technology modeled the dielectric behaviors of metal particle filled polymer composites operating under DC using OOF2 computer aided modeling. As a result, the giant permittivity phenomenon does not appear given the above assumption. Thus, it is concluded that the conductive particle filled polymer matrix does not exhibit the giant permittivity phenomenon under DC. Furthermore, the "apparent" giant permittivity observed under AC in aforementioned literatures may be distorted by eddy current loss during the permittivity characterization using the equivalent circuit model and not contribute to the enhancement of energy density.

2.9 Modeling

2.9.1 Eddy Current Loss

Eddy current loss P_e is proportional to the frequency ω:

$$P_e = K_e \omega^m \qquad 2.9$$

Where K_e is Eddy Current Loss constant, m is an exponential constant

In a recent study, Saito (2005) suggested that two mechanisms of eddy current loss exist in a conductive particle filled insulating matrix system, significantly affecting the value of exponential m:

a) Intra-particle Loss: when the conductive particles are well spaced and separated from each other, eddy current loss runs only inside particles, resulting in lower m value of 1.0 to 2.0. It suggests that at particle loading levels significantly lower than percolation threshold, the eddy current loss is small, shown in the lower part of Figure 14.

b) Inter-particle Loss: low insulation between particles causes low resistivity, and consequently eddy current runs between particles. In this case, eddy current loss is proportional to the square of the frequency (m=2). It suggests that near the percolation threshold, eddy current loss will substantially increase, shown in the upper part of Figure 14.

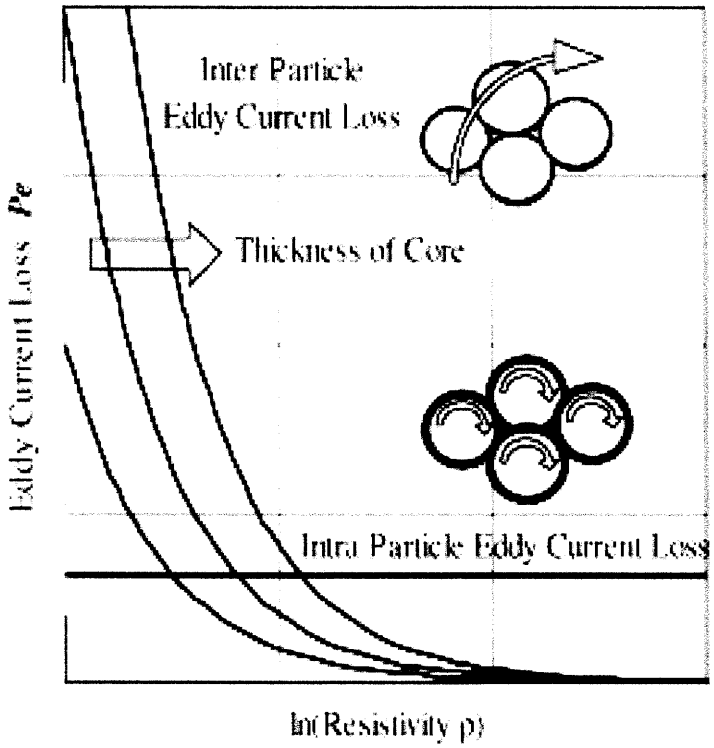

Figure 14: Relationship between resistivity and eddy current loss with two mechanisms of eddy current loss labeled (Saito 2005)

2.9.2 AC Permittivity

Most of the AC permittivity characterizations of electrochemical cells utilize the equivalent circuit model, including the giant permittivity literatures of Pecharroman and Moya (2000) and Isomil (2006). Based on the most frequently used Randles Model (Marsoukov and Macdonald 2005), at high frequencies, an ultracapacitor cell is converges to an equivalent circuit of Figure 15.

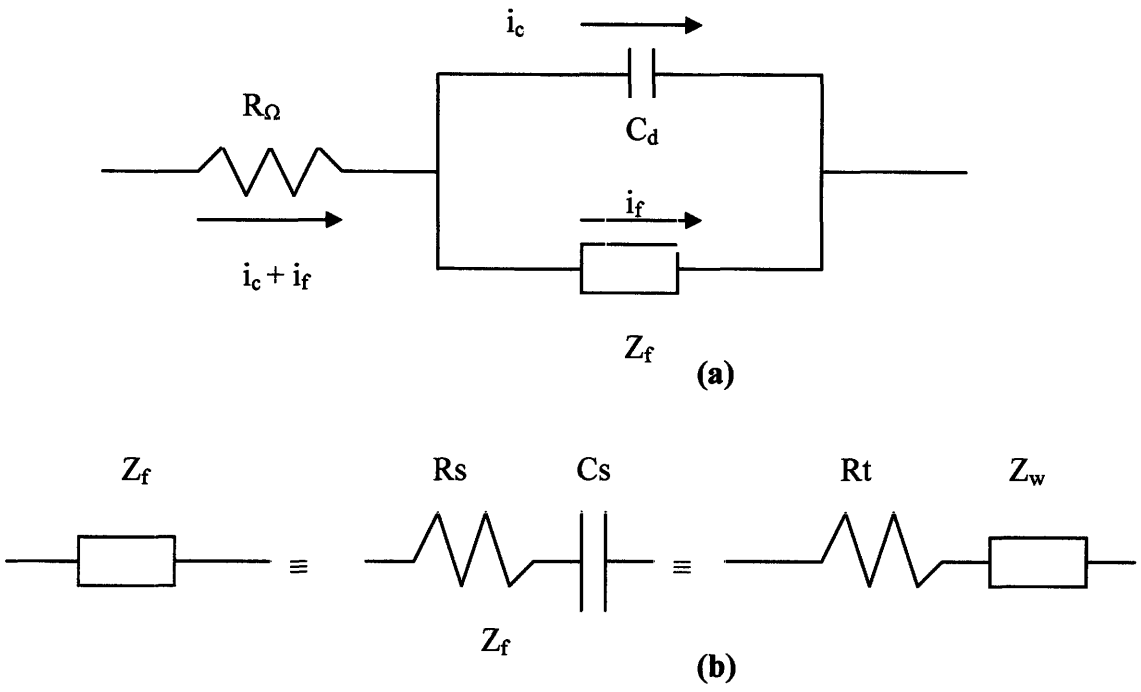

Figure 15: (a) Equivalent Circuit of an ultracapacitor cell, where i_f is the *current contributed from faradic process*, i_c is the *current contribution from double-layer charging*, C_d is the *double-layer capacitance* Z_f is a *general impedance* R is series of *solution resistance.* (b) Subdivision of Z_f into R_s, the *series resistance*, and C_s, the *pseudo-capacity*, or into R_{ct}, the *charge-transfer resistance*, and Z_w, the *Warburg impedance* (Marsoukov and Macdonald 2005)

The Randles Model describes the impedance as

$$Z = R_\Omega - j\left(\frac{R_{ct}}{R_{ct}C_d\omega - j}\right) \qquad 2.10$$

which consists of a real component and an imaginary component:

$$Z_{\mathrm{Re}} = R_\Omega + \frac{R_{ct}}{1+\omega^2 C_d{}^2 R_{ct}{}^2} \qquad 2.11$$

$$Z_{\mathrm{Im}} = \frac{\omega C_d R_{ct}{}^2}{1+\omega^2 C_d{}^2 R_{ct}{}^2} \qquad 2.12$$

The relationship between the system permittivity and the components of impedance is

$$\varepsilon = \frac{-Z_{\mathrm{Im}}}{(\varepsilon_0 \omega A/t)(Z_{\mathrm{Re}}{}^2 + Z_{\mathrm{Im}}{}^2)} \qquad 2.8$$

Rearrange Equations 2.8 – 2.12 and eliminate the components of impedance, we can obtain the relationship among system permittivity, applied frequency and components of the Randles Model:

$$\varepsilon = \frac{-\dfrac{\omega C_d R_{ct}{}^2}{1+\omega^2 C_d^2 R_{ct}{}^2}}{\dfrac{\varepsilon_0 A\left[(R_\Omega{}^2 + R_\Omega{}^2 \omega^2 C_d{}^2 R_{ct}{}^2 + R_{ct})^2 + \omega^2 C_d{}^2 R_{ct}{}^4\right]}{t(1+\omega^2 C_d{}^2 R_{ct}{}^2)^2}} \qquad 2.13$$

In order to observe the relationship between the permittivity ε and eddy current loss P_e, Equations 2.9 and 2.13 can be merged with the frequency term eliminated. As the purpose of this modeling is to observe the general trend of development, two simplifications are made: 1) assuming the eddy current loss to be proportional to ω^2 (m=2); 2) assuming a function Y monotonically and linearly increasing with P_e

$$Y = AP_e + 1 \qquad 2.14$$

With the above two assumptions, Equations 2.9 and 2.13 are then merged to give

$$\varepsilon = \frac{Y}{(R_\Omega{}^2 Y + R_{ct})^2 + (Y-1)R_{ct}{}^2} \qquad 2.15$$

Giving reasonable positive values to R_Ω and R_{ct} (Marsoukov and Macdonald 2005), Figure 16 plots Y versus ε, indicating the generalized relationship between the eddy

current loss and permittivity. Hence, based on the Randles Equivalent Circuit Model, the system permittivity generally increases rapidly with the increase of eddy current loss then plateaus off and becomes relatively independent of eddy current loss, which may indicate the insulation-conduction transition.

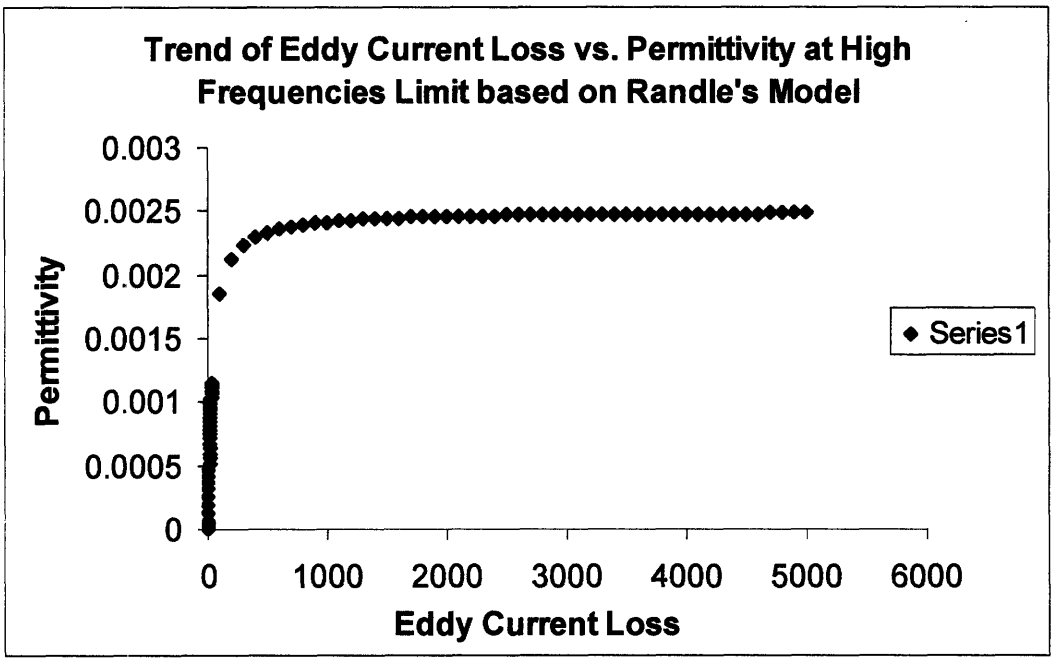

Figure 16: Trend of eddy current loss vs. permittivity at high frequency limit based on Randle's Model

To conclude, in a conductive particle filled polymer system, eddy current loss depends on the particle loading level and increases dramatically in approaching percolation threshold. In the AC permittivity calculation of a capacitor, equivalent circuit model is used and the magnitude of permittivity is found to increase rapidly with the increase of eddy current loss and hence the increase of particle loading level. As a result, the giant permittivity phenomenon observed under AC operation may only be "apparent" and could not contribute to the enhancement of energy density. At DC operation, this interference of the

permittivity from the eddy current loss diminishes and hence the apparent giant permittivity cannot be observed both from the experiments and modeling.

2.9.3 Particle Geometry

A more fundamental question to the energy storage mechanism in the OSSU model is whether the geometrical dispersion of conductive particles in polymer matrix would enhance the energy storage capability. A model has been developed to simulate such system, in which the periodic intervals of insulating polymer plates and conductive metallic plates are connected in series to represent the dispersion of conductive particles in polymer matrix as shown in Figure 17 (a). Thus, the model is equivalent to a number of identical capacitors connected in series shown in Figure 17 (b). Thus, if the volume of metallic phase remains constant, the finer the alternating plates are divided, the finer the particle dispersion the model represents. Further assumptions include:

1) The metallic volume fraction, f, remains the same
2) The voltage applied across the two electrodes remains the same, V_1
3) The polymer composition within capacitors remain the same, i.e. the dielectric constant of polymer, ε, remains the same
4) The total distance between the two electrodes, d, remains the same

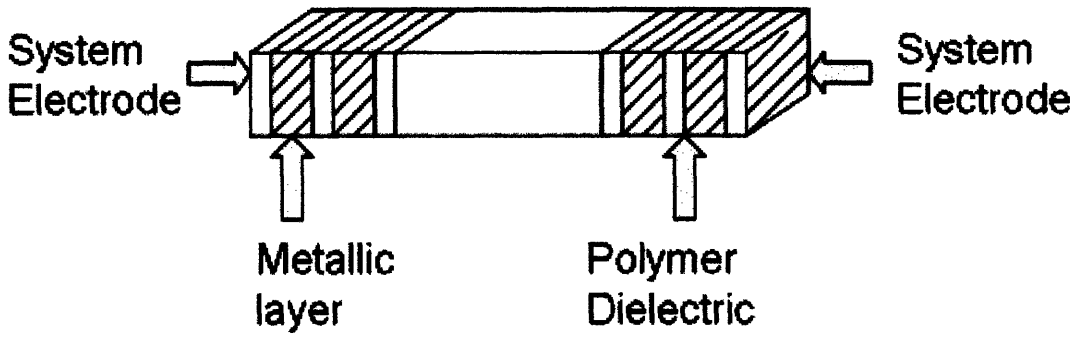

Figure 17 (a): Analogous geometric model for OSSU system: periodic intervals of polymer and metallic plates to form a number of capacitors in series.

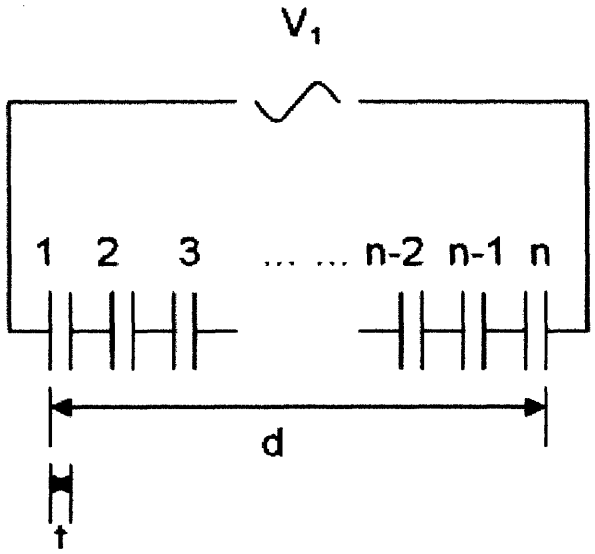

Figure 17 (b): Series of identical capacitors equivalent to Model 17 (a) where t is the distance between electrodes or thickness of polymer plate; d is total distance between system electrodes

From the previous knowledge, it is proved that

a) If n identical capacitors are put in series and subject to a total voltage of V_1, then the voltage across each individual capacitor is V_1/n

b) Assuming n identical capacitors put in series, if the capacitance of individual capacitor is C, then the total capacitance equals C/n

c) The total energy that can be stored in the system equals to the sum of the energy stored in each individual capacitor, $E=E_1+E_2+\ldots+E_n$

With n capacitors in series, the relationship between the energy storage capability and the number of capacitors in the system is presented as follows:

The thickness of a single capacitor is

$$t = \frac{(1-f)d}{n} \tag{2.16}$$

The voltage across the electrodes of a single capacitor is

$$V = \frac{V_1}{n} \tag{2.17}$$

The capacitance of an individual capacitor:

$$C = \frac{A\varepsilon_0\varepsilon}{t} \tag{2.18}$$

Combining Equation 2.16 and 2.18:

$$C = \frac{An\varepsilon_0\varepsilon}{(1-f)d} \tag{2.19}$$

Energy stored in a single capacitor:

$$E = \frac{CV_1^2}{2n^2} \tag{2.20}$$

Combining Equation 2.19 and 2.20:

$$E = \frac{V_1^2\varepsilon_0\varepsilon}{2(1-f)dn} \tag{2.21}$$

The Total Energy that can be stored for n capacitors in series:

$$E_t = nE = \frac{V_1^2 \varepsilon_0 \varepsilon}{2(1-f)d} \qquad 2.22$$

Thus, the energy stored in a series of capacitors satisfying above assumption is independent of the number of capacitors in series. Analogously, the geometrical dispersion of conductive particles in the polymer system generally does not contribute to the energy density enhancement.

2.10 Conclusion

1) Solid State Ultracapacitors (SSUs) enhances energy density by engineering dielectric materials to have high DC permittivity and breakdown voltage

2) Electrical Energy Storage Units (EESUs) have been reported to possess improved permittivity by using ferroelectric barium titanate as the basic dielectric material and improved breakdown strength by microstructure engineering the base powder. EESU is the most promising SSU model so far despite of substantial technology uncertainties.

3) Organic Solid State Ultracapacitors (OSSUs) proposes conductive particle filled polymers as the dielectric material. However, in the experiments and modeling, giant permittivity is not observed under DC. The apparent giant permittivity characterized under AC can be strongly distorted by the eddy current loss. Geometric model also suggests that the dispersion of conductive phase does not contribute to the energy density enhancement. Hence, it is concluded that OSSU is not a competitive SSU model.

Chapter 3 Performance and Market Analysis

3.1 Hybrid Electrical Vehicles (HEVs)

Hybrid Electrical Vehicles (HEVs) are vehicles powered by both electricity and gasoline. An HEV power system consists of an Internal Combustion (IC) engine, an electric motor, and an electrical storage system in a flexible architecture. The typical powertrain architecture of an HEV is shown in Figure 18 in which battery and IC engine can simultaneously or alternately power the vehicle in the most efficient way. Readers are suggested to familiarize some of the most constantly used terminologies in HEV technologies and performances in Appendix 1.

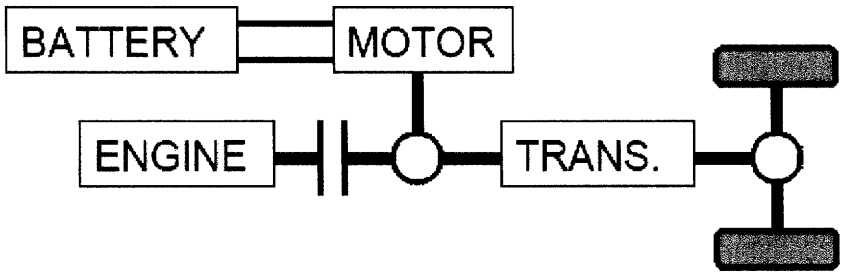

Figure 18: Parallel HEV powertrain architecture

A major performance advantage of HEVs compared with conventional liquid fuel powered vehicle is the fuel economy. Markel and Simpson (2006)'s research suggested that, for the equivalent performance on a mid-sized sedan, current HEV technology can achieve an average of 30% reduction in petroleum consumption compared with conventional automotives shown in Figure 19.

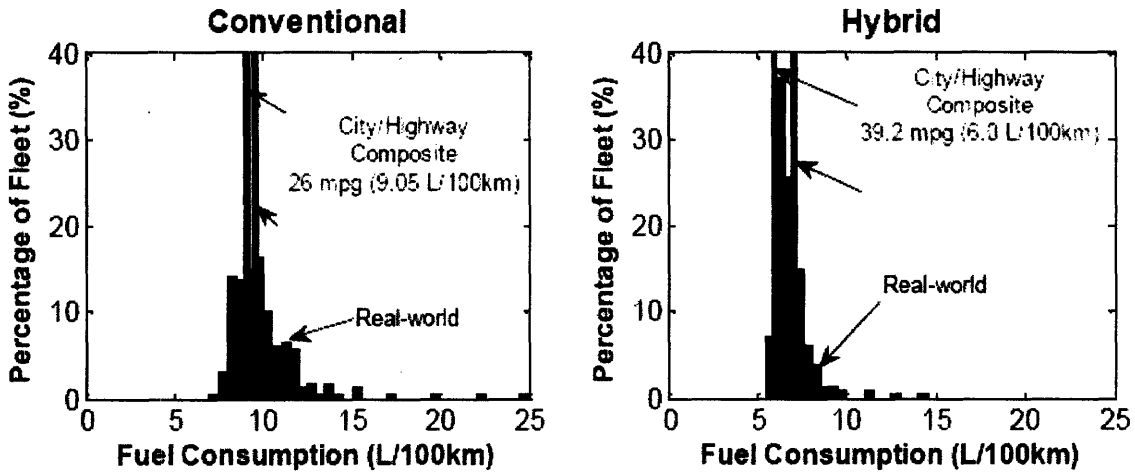

Figure 19: Comparison of fuel consumption statistics between conventional midsized sedan and HEV of equivalent performance (Markel and Simpson 2006)

The tradeoff of such fuel efficiency, however, is the incremental weight, volume and manufacturing cost of the powertrain. Figure 20 presents the cost breakdown of the powertrains on the conventional vehicles (VCs) and different types of hybrid electrical vehicles (HEVs). Currently, batteries are the major electrical energy storage device and dominate the incremental cost of HEV powertrain system. Technologically, the most maturely developed batteries for HEVs are Nickel Metal Hydride (NiMH) and Lithium Ion (Li-Ion) batteries due to their satisfactory service lifetime to sustain required SOC swing (Rosenkranz 2003). However, when the All-electrical Range (AER) of HEVs increases, the increased premium battery cost would offset the cost benefit from the higher fuel efficiency, such as in the case of PHEV20 and PHEV40. This cost deficiency based on the current battery technologies significantly hinders the commercialization of Plug-in Hybrid Electrical Vehicles (PHEVs), which leaves great market opportunities for

competitive technologies[8] such as Solid State Ultracapacitors (SSUs). The competition between the fuel efficiency and the incremental vehicle cost determines the market competitiveness of HEVs.

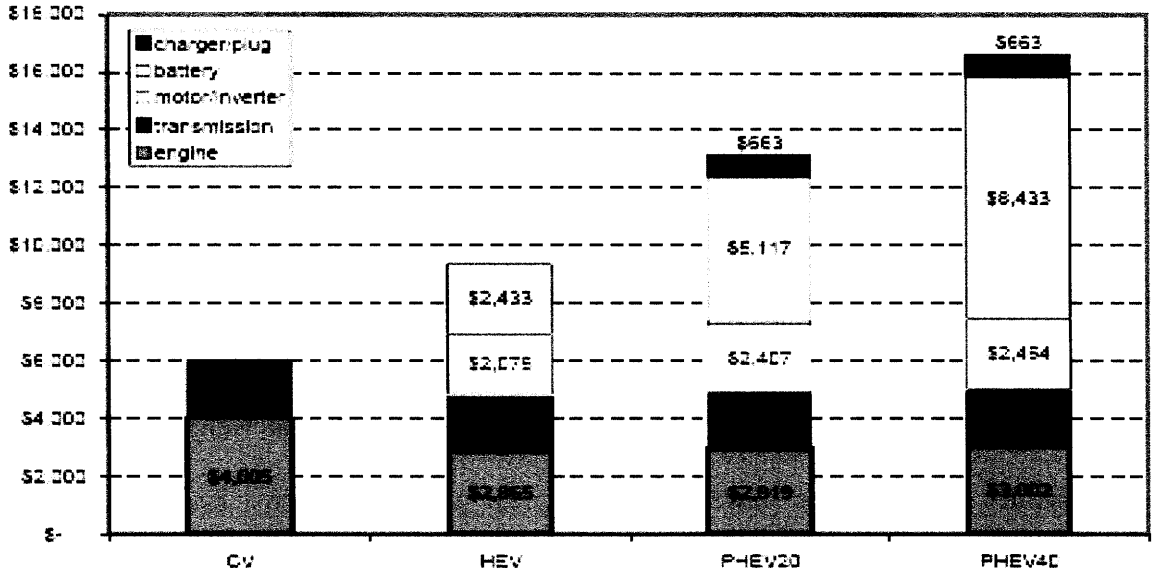

Figure 20: Cost breakdown of powertrain on conventional vehicle (CV), hybrid electric vehicle (HEV) and plug-in hybrid electrical vehicle (PHEV)

3.2 Overall Market Size Estimation for HEVs

The market demand of HEVs is very sensitive to the petroleum price and cost of electrical energy storage device. It is also affected by tax incentives, government regulations and eco-friendly consumer behaviors. Since the first market introduction of Toyota Prius in 1997, HEVs' global sales have experienced a steady annual growth at

[8] Electrochemical Capacitors (ECs) have some successful demonstrations but only limited to large vehicles in public transportation systems due to their limited energy density and requirements for frequent stop-recharging (Aowei 2007).

80%. Figure 21 shows the HEV sales volume in the US market from 2004 to 2007[9]. It is predicted that by the year 2015, the annual global sales of HEVs will reach 4.5 million units with a $6 billion market for the energy storage device (Pillot 2005). Figure 22 illustrate the trend of the market size prediction for the HEV battery market.

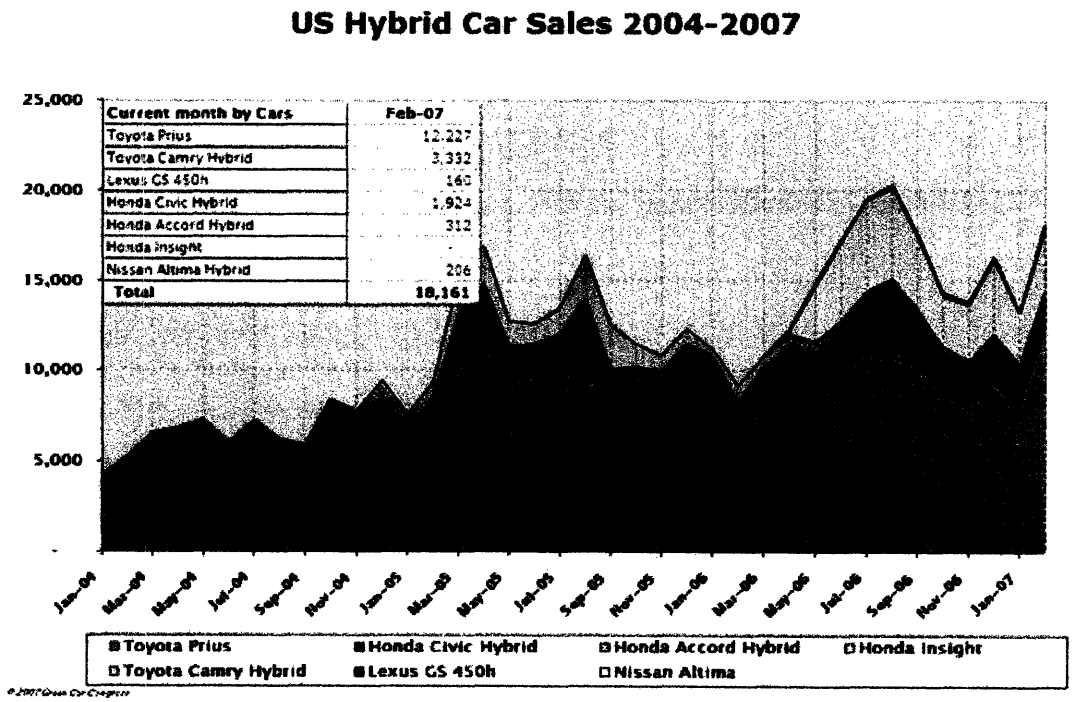

Figure 21: Hybrid Electrical Vehicle Sales Chart in the US market (Source: Green Car Congress 2007)

[9] Currently, the major manufacturers of HEVs in the US include Toyota, Honda, Ford and General Motor.

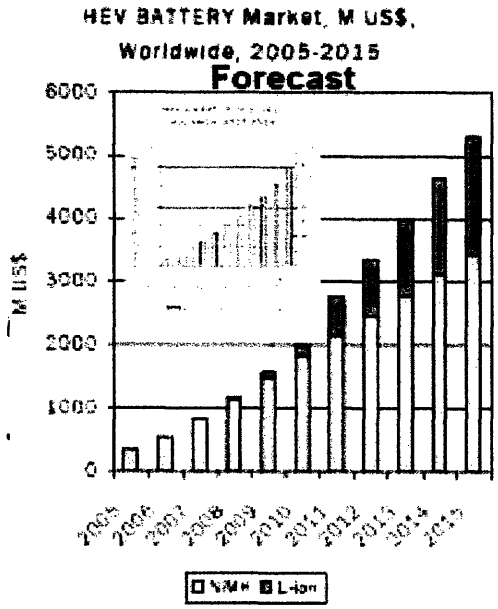

Figure 22: Global HEV battery market forecast from 2005 to 2015. (Pillot 2005)

In terms of demand sensitivity, Figure 23 (Frank 2007) shows how the fluctuation of gasoline price can affect the US consumers' choice among conventional vehicle (VC) and HEVs with different AERs: 15% more consumers would choose HEVs over VCs when the oil price increases from $1.65/gal to $3/gal, as it has been the case for the last five years (Figure 24). Among those 15%, more consumers would choose HEVs with higher AER due to more efficient fuel consumption.

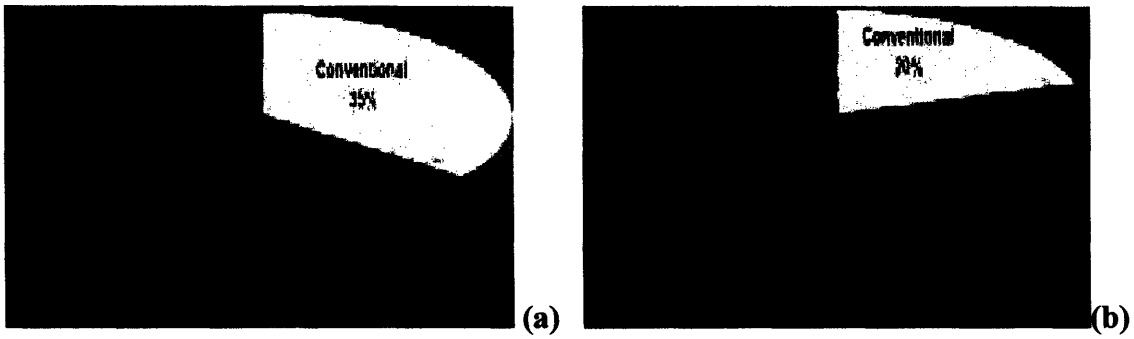

Figure 23: Market Preference when the gasoline price is (a) $1.65/gallon (b) $3.00/gallon (Frank 2007)

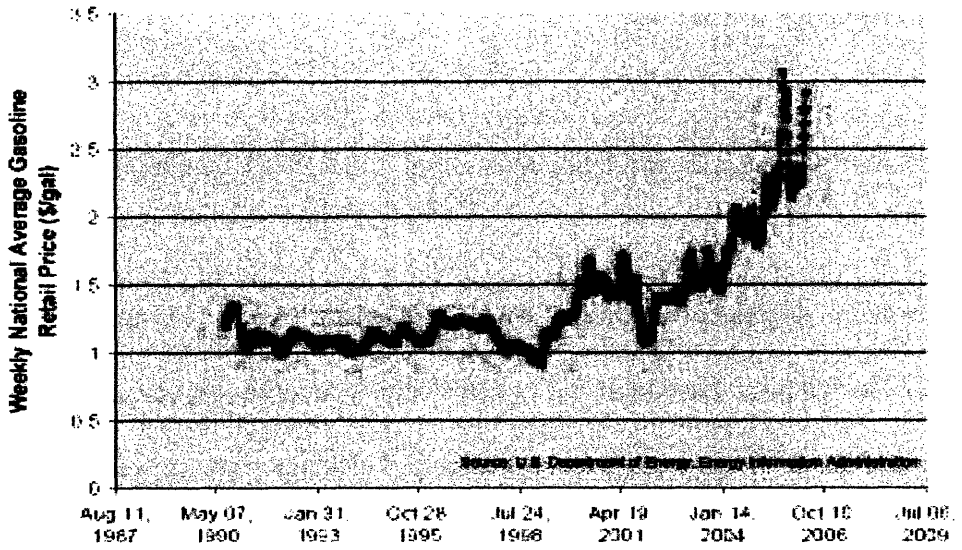

Figure 24: Weekly national average gasoline retail price from 1990 to 2007 (Gonder et al. 2007)

3.3 Plug-in Hybrid Electric Vehicle (PHEV)

A plug-in hybrid electric vehicle (PHEV) is an HEV with the ability to recharge its energy storage system with electricity from the electric utility grid. PHEVs have appreciable improvements in fuel efficiency compared with HEVs. PHEVs can reduce per-vehicle fuel use by up to 50% for PHEV20 and 65% for PHEV40 (Gonder 2007). Another key benefit of PHEV technology is that the vehicle is no longer dependent on a single fuel source. Renewable energies, including wind, solar, etc. can be used to power vehicles directly through PHEV's ability to recharge from the grid.

3.3.1 Fuel Efficiency of PHEVs

The reduction of per-vehicle petroleum consumption in a PHEV results from two factors:

1 Petroleum displacement during Charge Depletion mode (CD-mode), relating to the PHEV*x* designation based on the added battery energy capacity of the vehicle. Expanding CD-mode directly leads to increased fuel efficiency and powertrain cost.

2 Fuel-efficiency improvement in Charge Sustaining (CS) mode due to hybridization, which relates to the degree-of-hybridization (DOH) or added battery power capability of the vehicle. HEVs, which do not have a CD-mode, are only able to realize savings via this second factor.

For a PHEV*x*, these two factors can be combined mathematically as follows:

$$\frac{FC_{PHEVx}}{FC_{CV}} = [1 - UF(x)]\frac{FC_{CS}}{FC_{CV}} \qquad 3.1$$

Where FC_{PHEV} is the fuel consumption of $PHEV_x$, (gallons/mile)

FC_{CV} is the fuel consumption of conventional vehicle (gallons/mile)

FC_{CS} is the fuel consumption of charge sustaining mode (gallons/mile)

UF(x) is the utility factor (Figure 25), a value indicator of the fraction of total daily miles that are less than or equal to a specified distance based on typical daily driving behavior according to 1995 National Personal Transportation Survey. In the context of HEVs, it is

an effective utility measurement of AER to the US consumers, which will affect fuel efficiency and market demand of HEVs. Note that the utility curve resembles a parabolic relationship to the daily mileage, indicating the diminishing value of AER especially higher than 100 miles/day.

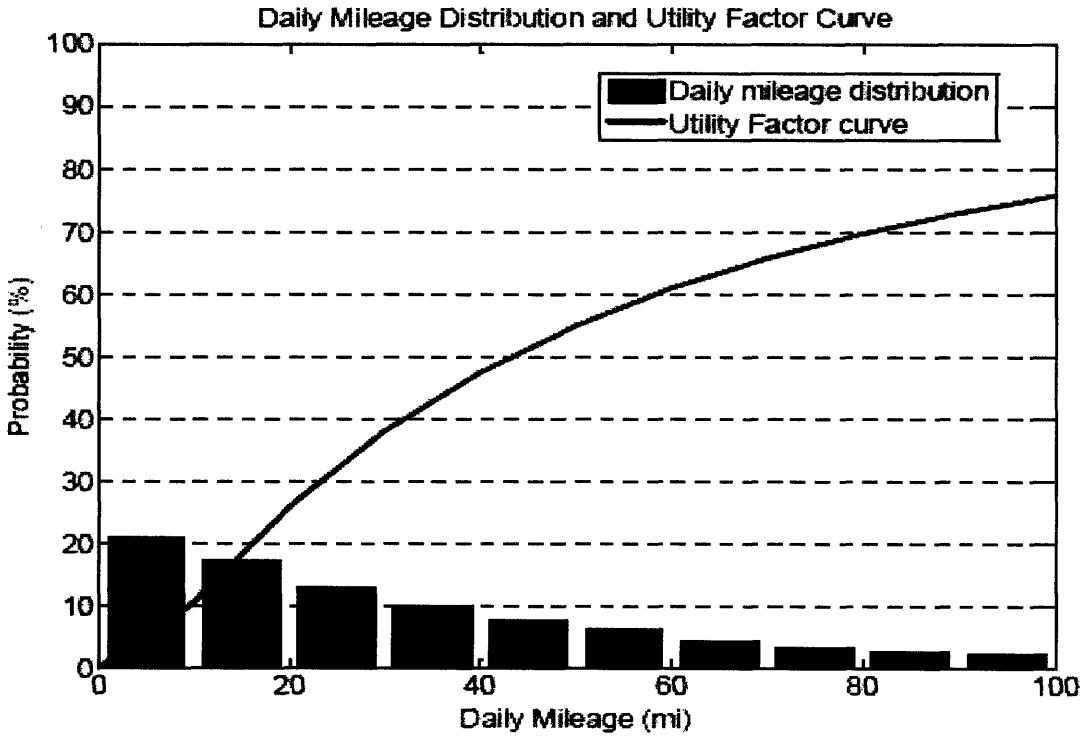

Figure 25: Daily mileage distribution and Utility factor curve (Simpson 2006 based on the 1995 National Personal Transportation Survey)

The overall fuel efficiency of a PHEV is a blended combination of the CD and CS-mode, which can be programmed to suit urban or highway driving schemes. Derived from Equation 3, Figure 26 is a plot of total petroleum reduction vs. petroleum reduction from the CS-mode for HEV0 and PHEVs with various AERs. The blended strategy opens up a spectrum of operation mode combinations for PHEVs. For example, a 50% of petroleum

reduction can only be achieved by an HEV0 operating CS-mode alone. To achieve the same fuel efficiency, a PHEV20 can choose to have 30% of fuel reduction from the CS-mode whereas a PHEV40 can choose to operate on CD-mode alone as shown in Figure 26.

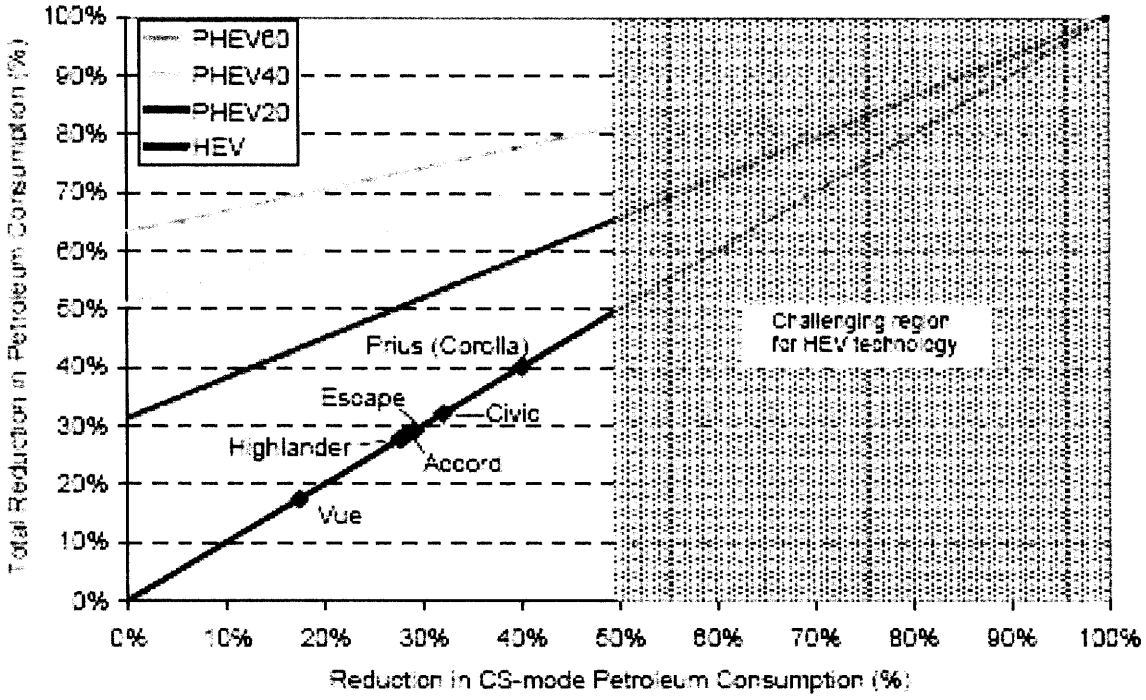

Figure 26: Potential per-vehicle reduction of petroleum consumption in HEV and series PHEVx (Gonder 2007)

3.3.2 Vehicle Cost of Current PHEVs

The major obstacle for the commercialization of PHEVs is the premium vehicle cost. Currently, a NiMH battery set for HEV0 costs $1000-2300/kWh. In addition, the battery cost increases with the increased power to energy (P/E) ratio. Gonder et al. (2007) presents such relationship Figure 27.

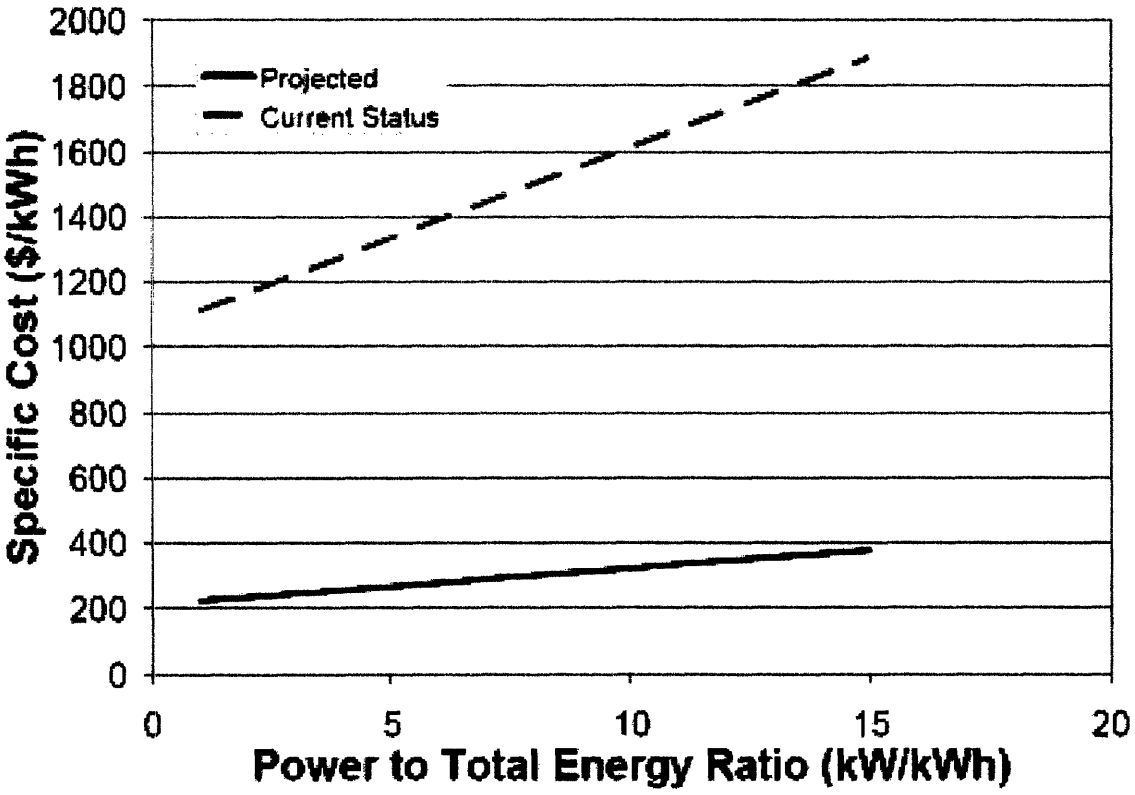

Figure 27: Typical specific cost of energy storage systems (Markel and Simpson 2006)

Currently, the incremental battery cost negatively affects the market competitiveness of PHEVs despite of PHEVs' superior fuel efficiency. Simpson (2006) estimates that, on average, for a PHEV to provide financial payback relative to a hybrid electric vehicle within 10 years, battery costs must reach long-term, high-volume cost estimated to be less than $300/kWh, and gasoline costs must increase to more than $4/gal. In the absence of both lower battery costs and higher gas prices, alternative value propositions (e.g., government incentives, vehicle-to-grid revenue, battery leases, the value of a "green" image, etc.) must be considered to overcome the cost premium of PHEVs. These financial and technology uncertainties provide opportunities for alternative electrical energy storage systems.

3.4 Solid State Ultracapacitor (SSU) HEVs

Solid State Capacitors (SSUs), due to the reported higher energy and power density, longer service life and economic manufacturing, have the potential to replace batteries to become the primary electrical energy device in HEVs and PHEVs. It is expected that an SSU equipped HEVs or PHEVs would have higher driving power, faster recharging, expanded AER, increased degree of hybridization (DOH), better energy efficiency and longer service life than battery HEVs or PHEVs. The following sections will introduce PHEV models with Electrical Energy Storage Unit (EESU) as the electrical energy storage device. The PHEV performance model is based on milestone reports of National Renewable Energy Laboratory and the EESU performance data is projected from the materials property estimation given the physical origin of energy storage and basic structure of EESU introduced in Section 2.5.

3.5 Potential Advantages of EESU PHEVs

Economic Vehicle Cost

Weir (2006) claimed that the manufacturing cost of EESU would be competitive to that of lead acid battery based on the inexpensive raw materials and relatively matured production process.

Enhanced Power Density

Due to the higher power density of ultracapacitors, an EESU PHEV will have much higher power output from the electric motor than a battery equipped PHEV, which would solve a major issue of current HEVs. The higher power density also significantly shortens the charging time. According to Weir (2001)'s claim shown in Table 2, to fully charge an EESU will be at least 15 times faster than a conventional NiMH battery with the same energy capacity. This time efficiency would substantially reduce the complication of maintenance, making an EESU PHEV more driving friendly.

Vehicle Range Extension

The higher energy density of EESU will substantially increase the electrical energy storage capacity, which, in turn, enhances the AER of a PHEV. According to Weir (2001)'s patent, a 336lb of EESU with the claimed energy density of 280 Wh/kg can achieve an AER of 300 miles. This strategic advantage leads to enhanced operation mode flexibility and fuel efficiency.

Expansion of CD and CS-Mode Operation Window

Due to the extended AER brought by EESU, the energy consumption strategy can have a more flexible window of mode control. For instance, the improved AER can have a direct positive impact on the petroleum reduction in CD-mode.

Fuel efficiency

The increased electric driving capacity and the further optimized driving mode operation would invariably lead to the improved fuel efficiency.

3.6 Performance Modeling of EESU PHEVs

The optimistic performance predictions of EESUs as the major electrical energy storage device in new generations of HEVs have drawn much attention in the automotive industry. However, no research other than EEStor Inc. so far has analyzed the potential performance and financial viability of EESU in a quantitative manner. This section will present an EESU PHEV performance model in energy consumption, manufacturing cost and financial uncertainties in comparison with the currently existing battery equipped PHEVs.

3.6.1 Energy Consumption Model of EESU PHEVx

Due to the potentially superior energy density, the All Electric Range (AER) of EESU equipped PHEVx could be substantially higher than that of battery equipped PHEVs. Modeling of petroleum and electricity consumption of EESU PHEVs can help to establish:

1) Fuel efficiency and driving economy of EESU PHEVs
2) Cost and benefit analysis of commercializing EESU PHEVs
3) Driving profile optimization
4) Market demand estimation of EESU PHEVs

Previous studies (Simpson 2006, Gonder 2007) suggested that the fuel efficiency estimation can be more accurately obtained by modeling PHEVs petroleum and electricity consumption separately. This research will adopt this method.

Petroleum Consumption

Petroleum consumption, according to Equation 3.1 in Section 3.3.1, is a function of utility factor (UF) and fuel consumption rate of CS-mode. Markel and Simpson (2006)'s study estimated that in recent PHEV technologies, CS-mode fuel consumption rate stands around 0.027 gallons per mile, which is relatively independent of the energy storage capacity of the storage device. The utility factor of EESU was modeled in Simpson (2006)'s research shown in Figure 25. Thus, the average fuel consumption (gallons per mile) for PHEV is

From Equation 3.1:

$$FC_{PHEVx} = [1 - UF(x)]FC_{CS} \qquad 3.2$$

Assume FC_{CS} = 0.027 gallons per mile, then

$$FC_{PHEVx} = 0.027[1 - UF(x)] \qquad 3.3$$

Electricity Consumption

Based on Simpson (2006)'s research statistics of various PHEVx operating at optimum DOH in the near term, the electricity consumption for PHEVx is projected as a function

of x (AER) in Figure 28. Hence, the Electricity Consumption Rate (ECR, Wh/mile) bears the following relationship with the AER range (x) of PHEVx:

$$ECR_{PHEVx} = 6.6774x^{0.8691} \quad 3.4$$

Average Driving Efficiency (ADE)

Thus, the Average Driving Efficiency (ADE, cents per mile) can be estimated by combining Equation 3.3 and 3.4:

$$ADE = gas\_price * FC_{PHEVx} + elec\_price * ECR_{PHEVx} \quad 3.5$$

$$ADE = gas\_price * 0.027[1 - UF(x)] + elec\_price * 6.6774x^{0.8691} \quad 3.6$$

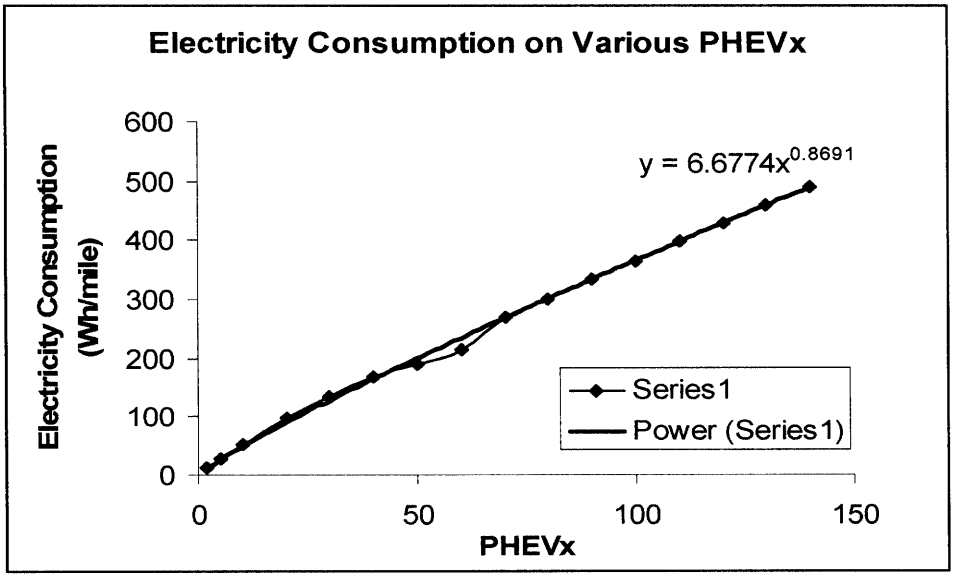

Figure 28: Average electricity consumption on various PHEVx. Data points beyond PHEV60 are projected from the trend of Simpson (2006)'s statistics under PHEV60

Note that the above model is a fairly conservative estimation because 1) the model adopts the increase trend in curb mass with the AER range as in battery PHEVs. The curb mass of an EESU PHEVx, however, is substantially less than that of battery PHEVx with the same AER, which significantly saves the additional cost both to power and re-design the vehicle, 2) the model assumes relatively low degree of hybridization[10] (DOH) based on the existing batteries models, the actual DOH can be much higher since EESUs could have much larger SOC window with very limited service life deterioration, which, in turn, substantially enhances fuel efficiency.

3.6.2 Case Study of EESU PHEV140

This case study is a set of performance comparisons between a Li-Ion battery PHEV40 and EESU PHEV140 for a midsized sedan due to their similar weight and volume. Based on released EESU specifications (EEStor 2007), if we assume an EESU device to occupy the similar volume (15L) as today's Li-Ion battery pack in a PHEV40 (A123 Systems 2007), EESU would be slightly lighter than the Li-Ion battery pack (130lb instead of 150lb), with AER of 140 miles, corresponding to a utility factor (UT) of 0.82. Based on the established fuel consumption model, the following calculations characterize some important performance parameters:

[10] DOH is defined as the ratio of motor power to total motor plus engine power (NREL 2007).

Fuel Efficiency

From Equation 3.1:

$$\frac{FC_{PHEV140}}{FC_{CV}} = [1 - UF(x)]\frac{FC_{CS}}{FC_{CV}} \qquad 3.7$$

$$FC_{PHEV140} = [1 - UF(x)]FC_{CS} \qquad 3.8$$

We know from the Utility Factor curve of Figure 25:

$UF(140) = 0.82$

And:

$$FC_{CS} = \frac{1}{mpg_{CS}} = \frac{1}{37mpg} = 0.027 gallons / mile$$

Then fuel consumption rate of a PHEV140 is

$$FC_{PHEV140} = 0.18FC_{CS} = 0.00486 gallon / mile$$

Thus the fuel efficiency of PHEV140 is $1/FC_{PHEV140} = 206$ miles per gallon.

Average Driving Efficiency (ADE)

At the targeted AER of 140 miles, the average electricity consumption rate for a PHEV140 is projected to be around 490 Wh/mile. Based on the constant electricity retail price of \$0.09 per kWh and the gasoline price of \$3 per gallon (EIA 2007), the average

fuel cost of an EESU PHEV140 is predicted to be 4.5 cents per mile, which indicates at least 20% of increase in energy efficiency than a battery equipped PHEV40 and over 60% of increased efficiency than a conventional vehicle (Markel and Simpson 2006)

Degree of Hybridization (DOH)

Based on Weir (2001)'s patent, an EESU equipped PHEV140 can provide motor power of around 140 hp. A midsized sedan requires the drivetrain power around 210 hp (Toyota Camry) to 240 hp (Buick Lacrosse). Thus an EESU PHEV140 can have up to 67% of DOH, almost 100% of increase compared with a Li-Ion battery PHEV40.

Cumulative Vehicle plus Energy Cost

Cumulative vehicle plus energy cost is a determinant parameter in comparing different types of HEVs, from which the energy payback time can be inferred. Information about the manufacturing cost of EESUs has been very limited due to technology immaturity and proprietary reasons. EEStor (2007) reported the unit cost of EESUs to be $0.85/Wh, similar to that of lead acid batteries and more economic than that of NiMH batteries (~$1.00/Wh) and electrochemical capacitors (ECs) (~$4.00/Wh) (Linden and Reddy 2001). Here, we conservatively estimate the manufacturing cost of EESU to be 50% of Li-Ion battery of the same weight. For instance, figure 29 shows the cumulative cost comparison among conventional vehicle (CV), Li-Ion HEV0 and HEV40 and EESU PHEV140 at current energy cost. The retail price of a Li-Ion HEV40 is predicted to be $35,000, an increment of $12,000 on the top of a conventional sedan, whereas an EESU PHEV140 is estimated to cost $29,000, an increment of $6,000.

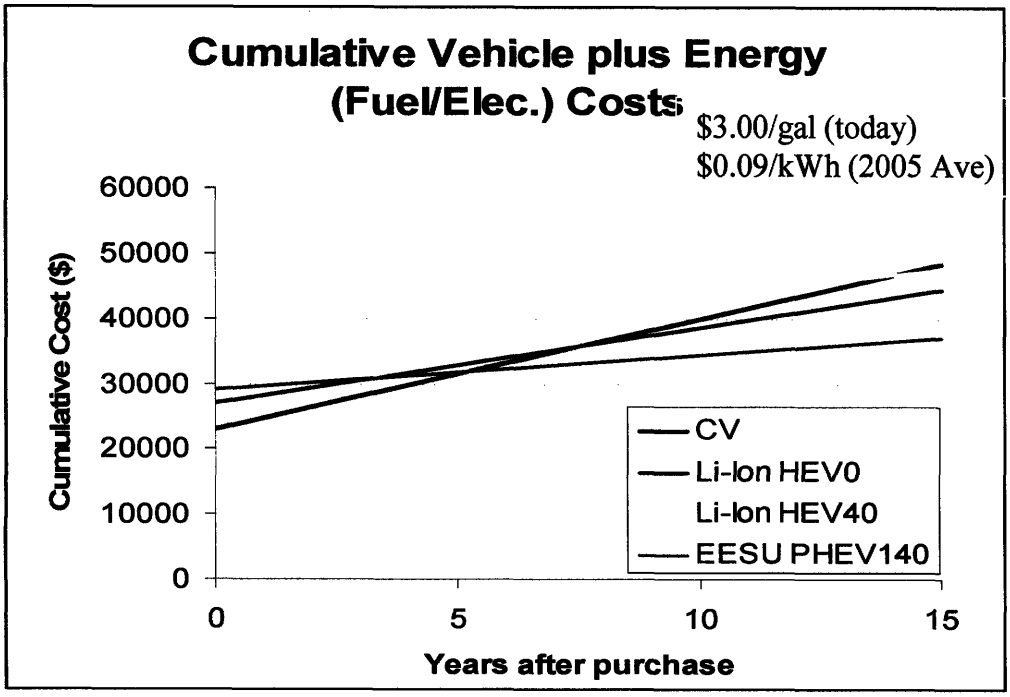

Figure 29: Cumulative cost comparison among conventional vehicle, Li-Ion HEV0, Li-Ion HEV40 and EESU PHEV140 at current energy price

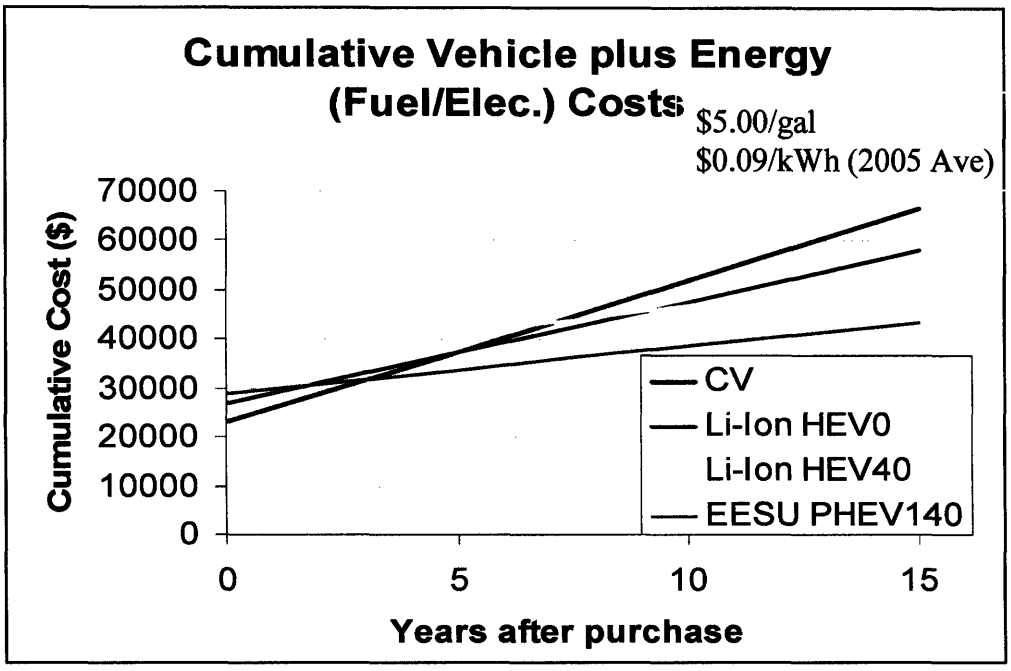

Figure 30: Cumulative cost comparison among conventional vehicle, Li-Ion HEV0, Li-Ion HEV40 and EESU PHEV140 at gasoline price of $5.00/gallon

Energy Payback Time

Based on the NREL data (Simpson 2006) of average driving efficiency (ADE) of different HEV models, estimated HEV vehicle cost and our previous conclusion that the energy consumption rate of an EESU PHEV140 is at least 20% less than an HEV40 and 60% less than a Conventional Vehicle (CV), we can characterize the energy payback time of EESU PHEV140 by plotting accumulative vehicle and energy costs for Conventional Vehicle (CV), Li-Ion Battery HEV0, Li-Ion Battery HEV40 and EESU PHEV140 in Figure 29 and 30. At the current energy cost, i.e. $3/gallon of gasoline and $0.09/Wh of electricity, the energy payback time of EESU PHEV140 would be five years compared to a CV, two years compared to an HEV0 and 0 years compared to an HEV40. If the gasoline costs $5/gallon, the energy payback time of EESU PHEV140 would be three years compared with a CV and one to two years compared with an HEV0.

3.7 Financial Uncertainties for EESU

Financial uncertainties of EESU equipped PHEVs would mainly come from the uncertainties in energy price and technology immaturity affecting the vehicle performance. The introduction of an ultracapacitor into the powertrain may complicate the design of vehicle and thus increase the cost. Although Feel Good Cars Inc. has purchased license from EEStor to produce EESU equipped electrical vehicles and planned to make them roadworthy in 2008. The automotive industry may still be very conservative to adopt such technology when a successful prototype has not yet been available.

Chapter 4 Startup Manufacturing Plan of EESU

In this chapter, a startup manufacturing plan for EESUs will be proposed for the year 2011 to 2020 with Period I from 2011-2015 and Period II from 2016-2020. This plan aims to provide a dynamic financial analysis to maximize profitability and minimize financial risks in response to the market unpredictability. At the end of this chapter, the initial investment, pricing and manufacturing strategies will be suggested in order to maximize expected Net Present Value (NPV) and minimize financial risks.

4.1 Business Model

The primary business model is to manufacture EESU components with the available base powders and other raw materials outsourced in the global market instead of conducting HEV system integration downstream. Hybrid Electrical Vehicle manufacturers have been identified as the primary customers for EESU components due to the tremendous market potential. EESUs also have the potential to replace batteries and electrochemical capacitors (ECs) as clean energy storage device (solar, wind, etc.) and temporary power replacement facility (e.g. secondary power in hospital). Thus, choosing to manufacture EESUs will ensure customer diversification and minimized financial risks while a strong market demand from the automotive industry is maintained. Due to the diminishing AER value discussed in Section 3.3.1, the first generation of EESUs will meet the requirement of a PHEV140.

4.2 Cost Analysis

For the first generation of EESUs, A cost model has been developed to take in consideration of the variable cost (raw materials, utility, etc.) and the fixed cost (land, equipment, etc.) as presented in Appendix 2. For both Period I and Period II and regardless of production volume, the raw materials [11] cost contributes the largest proportion of the expenditure, accounting for about 50% of the unit cost. The next largest cost comes from the electricity consumption due to the heat treatment requirement to process EESUs. A typical cost breakdown analysis is shown in Figure 31 for different manufacturing capacities running at full capacity utilization [12]. Because the main expenditure comes from the raw materials cost and electricity consumption, the resultant unit cost ($/kWh) is largely dependent on the variable cost. Thus, the potential for the economy of scale is predicted to be limited at different production volumes due to the relatively small contribution from the fixed cost. The extent of the economy of scale is detailed for the different production volumes shown in Appendix 3.

[11] The raw materials cost data is based on US. Geological Survey 2007, the major raw materials cost: pure Barium Titanate Powder $13.6/lb, Nickel $14.5/lb (USGS 2007)

[12] Full capacity utilization assumes the actual production volume equals the setup production capacity

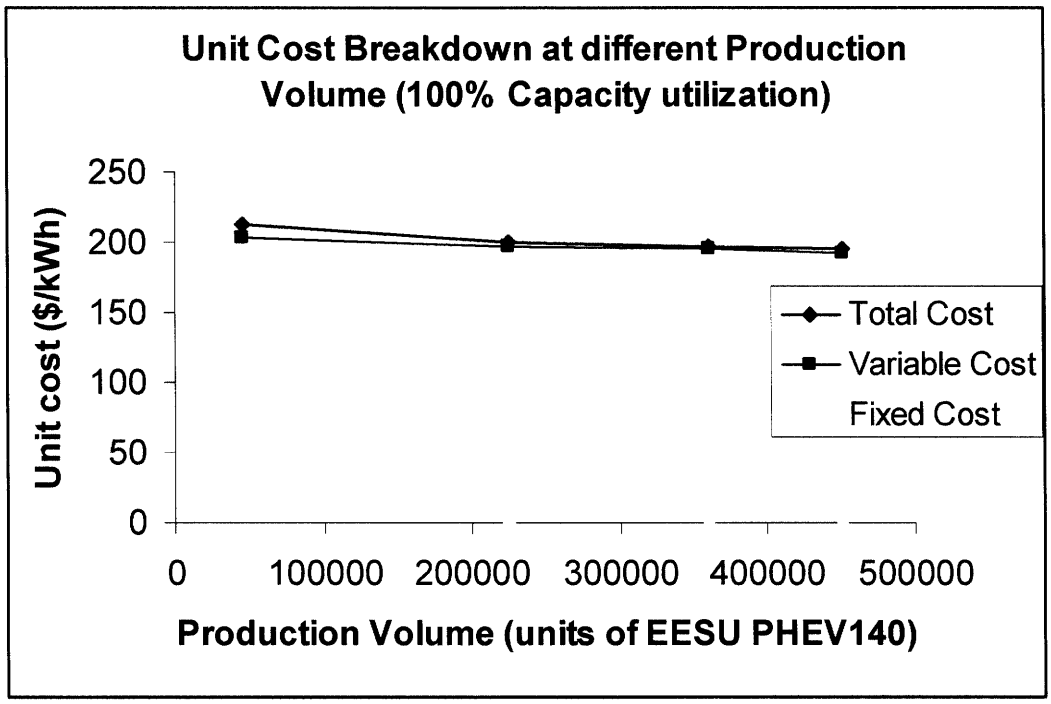

Figure 31: Unit Cost Breakdown at different production volume, assuming each manufacturing size is running at full capacity utilization

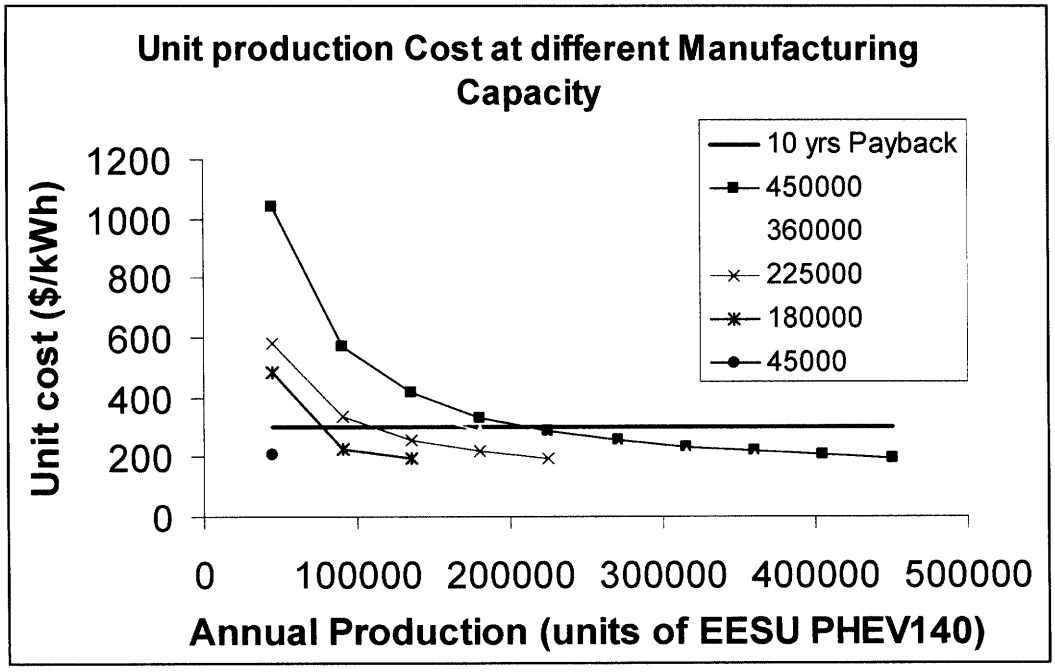

Figure 32: unit production cost at different manufacturing capacity, assuming different extents of overcapacity

Figure 32 shows the relationship between unit cost ($/kWh) and manufacturing capacity. The black horizontal line indicates a target long-term unit cost of $300/kWh set by Simpson (2006)'s research as the benchmark for a ten years payback economy[13] for a battery equipped PHEV relative to a HEV0. Having a unit price above this benchmark inevitably reduces the economic competitiveness of EESUs, leading to lower market share. As each family of data on Figure 32 suggests, the unit cost of EESU generally decreases when annual production volume approaches the designed manufacturing capacity. Hence, the risks of more than 50% of overcapacity[14] at different manufacturing capacities can potentially lead the unit costs into the financially unfavorable regions due to investment idling. The following analysis will concentrate on the methodology to mitigate this risk and present a plan to maximize expected value of investment.

4.3 Demand Analysis

Product demand analysis is based on two factors: the total potential market size and the potential market share. The total market size for EESU PHEVs can be estimated as a reasonable proportion of the market size of the HEV electrical storage device. In Pillot (2006)'s research, it is suggested that by the year 2015, the annual sale of all kinds of HEVs is projected to be 4.5 million units, equaling a market of more than $6 billion for the electrical energy storage device. Within this market, this report assumes the EESUs' share of electrical energy storage device depends solely on the product performance competitiveness which can be quantified by the product utility analysis.

[13] As introduced in Section 2.6.2, the ten years payback economy suggests the total vehicle and energy cost of a PHEV will become economically favorable compared with a current HEV0 in ten years

[14] Over capacity indicates the scenario where the actual production volume is less than the setup capacity

4.3.1 Product Utility Analysis

The product utility analysis is designed to assess the competitiveness of EESU from the customers' point of view, which, in turn, facilitates the forecast of market demand. The product utility is a comprehensive function of several performance attributes. As discussed in Section 3.2, the most determining criteria for PHEV performance are vehicle cost and fuel efficiency. Therefore, specific electrical storage device cost ($/kWh) and the utility factor of AER are the most representative attributes for the two criteria, respectively. The two attributes first independently form single utility functions:

i) The utility of electrical storage device cost is benchmarked by long-term specific battery cost analysis in Markel and Simpson (2006)'s research;

ii) The utility of AER is determined by the utility factor curve (Figure 25) in National Personal Transportation Survey 1995.

Then, the two independent functions, according to their weighted importance, form a two dimensional function to represent multi-attribute utility of an electrical energy storage device, shown in Appendix 4. Hence, quantitative comparisons between any two points within this bi-attribute space can be made to set the market strategy in response to the competition and demand.

4.3.2 Pricing Strategy and Market Demand Prediction

Period I (2011-2015)

If we assume the long-term target of PHEV batteries (Simpson 2006) to be EESU's competition, the competition benchmark is thus a PHEV40 with a specific battery cost (market price) of $300/kWh (Attribute 1) with an AER of 40 miles (Attribute 2), which gives the multi-utility of 0.438. Two representative prices and corresponding market demand scenarios for Period I are suggested with their multi-utility comparison illustrated Figure 33:

a) In order to gain more market penetration upon the market debut of EESU PHEV140, a lower specific EESU price can be set to be $245/kWh, giving a utility much higher than the competition (0.82 vs. 0.438). As a result, the probabilities of having a high market demand (2% HEV market size), medium demand (1% of HEV market size) and low demand (0.1% of HEV market size) are 35%, 35% and 30%, respectively (P_{high}: P_{med}: P_{low} = 35:35:30).

b) A higher price of EESU can be set to be $270/kWh without significantly compromising EESU's utility (U~0.72). In this scenario, the probability of having a high market demand is decreased to 15% and that of having low demand is increased to 50% (P_{high}: P_{med}: P_{low} = 15:35:50).

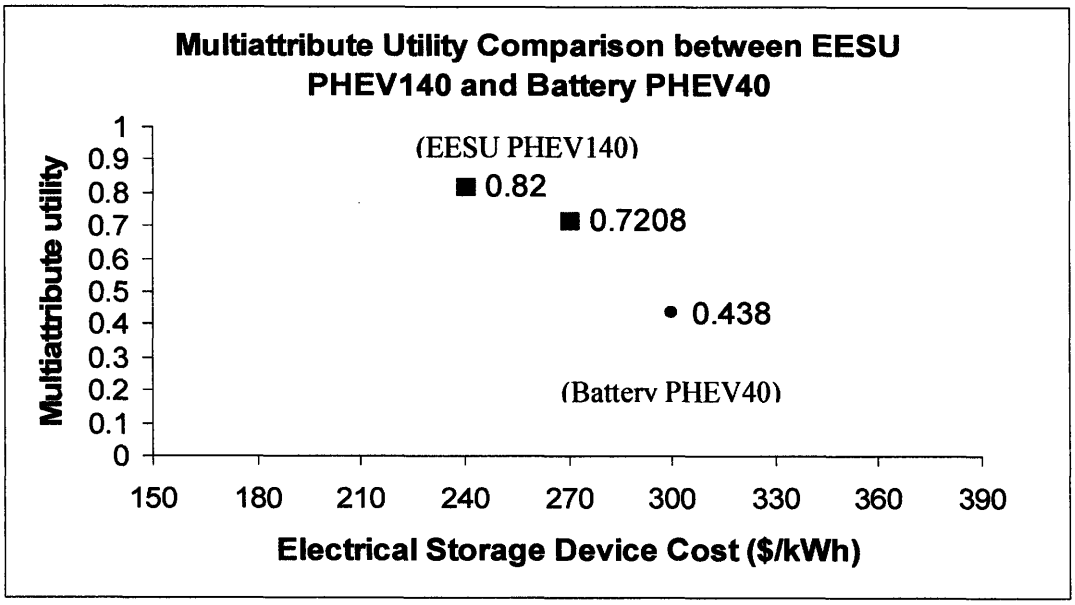

Figure 33: Multi-attribute utility comparison between EESU PHEV140 and Battery PHEV40 at different pricing scenarios

Period II (2016-2020)

As shown in Table 6, assuming the same pricing strategy, the market demand predictions in Period II are based on the actual demand outcomes of Period I. For instance, if the market growth of Period I is low, then in Period II, the probabilities of having a low demand are 50% and 70% for Price 1 ($240/kWh) and Price 2 ($270/kWh), respectively.

Table 6: Market Demand Predictions in Period II

Growth in Period I	**low**	**low**	**medium**	**medium**	**high**	**high**
Period II	Prob P1	Prob P2	Prob P1	Prob P2	Prob P1	Prob P2
low	50.00%	70.00%	10.00%	20.00%	20.00%	30.00%
medium	30.00%	20.00%	50.00%	70.00%	20.00%	40.00%
high	20.00%	10.00%	40.00%	10.00%	60.00%	30.00%

Note: P1 and P2 stand for Price 1 ($240/kWh) and Price 2 ($270/kWh), respectively

4.4 Proposed Manufacturing Strategy

In the Period I (2011-2015), the market analysis predicts the first year (2010) EESUs market share (to the manufacturer) within the HEV sector to be 0.1% (4,500 units) in case of low market demand, 1% (45,000 units) in case medium market demand and 2% (90,000 units) in case of high market demand[15]. The annual market share growth rate ranges from 2% to 11%, proportional to the market demand. The starting market share of Period II (2016-2020) is based on the resultant market share of at the end of Period I, with the similar trend of annual growth rate (2%-11%) in the subsequent years. At the beginning of each period, decision is made as to choose the optimal plant size to maximize expected NPV in response to the market demand. The model eliminates the choices of plant size into three options to accommodate the three scenarios in the market demand prediction: 4881 units/year for a small scale site, 54762 units/year for a medium scale site and 136905 units/year for a large scale site.

Using the dynamic accounting model developed by Roth et al. (1994) based on expected value maximization and 15% of annual discount rate, Table 7 presents the computed results of the optimal dynamic pricing and plant expansion strategies rendering the maximized expected NPV of $83 million.

[15] This estimation is based on the similar trend of HEV's market acceptance rate in the first five years since HEVs introduction in the US market, according to the statistics of US Department of Transportation (2004).

Table 7: EESU Pricing and Plant Expansion Strategy Summary

Period I (2011-2015)	
Scale	Small Scale
Price	Price 1
Period II (2016-2020)	
Low Demand in I	Do Nothing/Close
Medium Demand in I	Medium Scale; Price 2
High Demand in I	Large Scale; Price 2
EV (NPV)	$83,154,126

From the computed results, in Period I, the small scale plant size and Price 1 ($245/kWh) are chosen. What's worth noticing is that none of the pricing and plant size combination will give a positive expected NPV in Period 1 due to the large initial investment and limited market penetration. However, the optimal combination of small scale plant size and lower price strategy minimizes expected lost, although there are probabilities of profit generation if other strategies were chosen. For instance, Figure 34 (a) illustrates the cumulative profits for three different market demand scenarios in Period I if the optimal strategy is chosen, in which the small manufacturing scale cannot achieve sufficient economy of scale to generate positive profit margin in all scenarios. Figure 34 (b), on the other hand, shows the cumulative profits at Price 1 ($245/kWh) if a medium plant size is chosen. There is 30% of probability (high demand) that the profit can be generated from the first year of operation due to the economy of scale. There is also 35% of probability (medium demand) that a breakeven can be achieved between 2013 (3rd year) and 2014

(4^{th} year). However, the probability of suffering from huge financial lost ($750 million by 2015) due to overcapacity in case of low demand is too high to ignore (35%), which significantly reduces the expected NPV in this financial model.

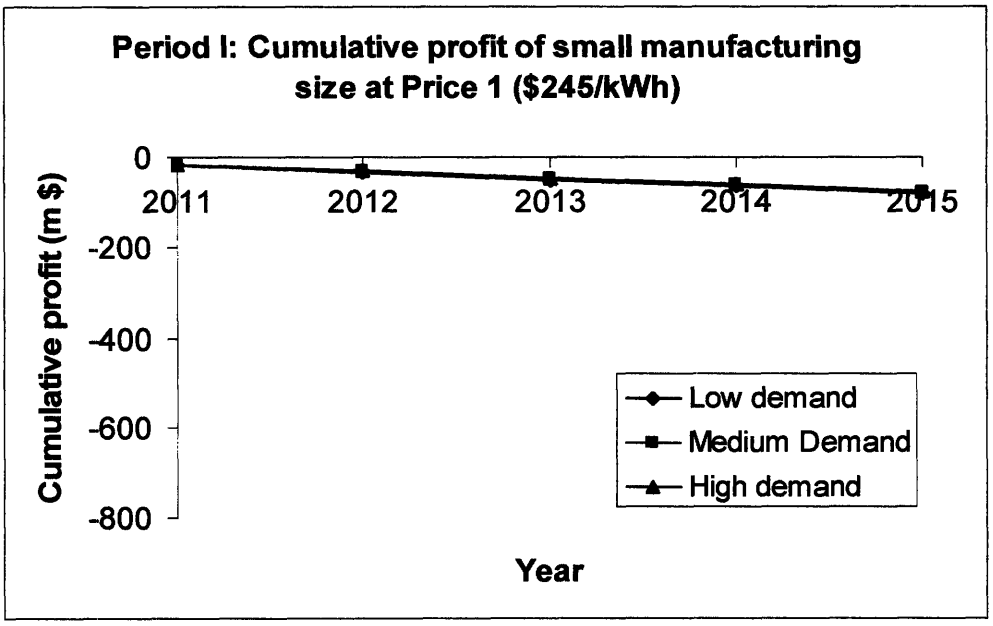

Figure 34 (a): Cumulative profit of small manufacturing size at Price 1 for different market demands

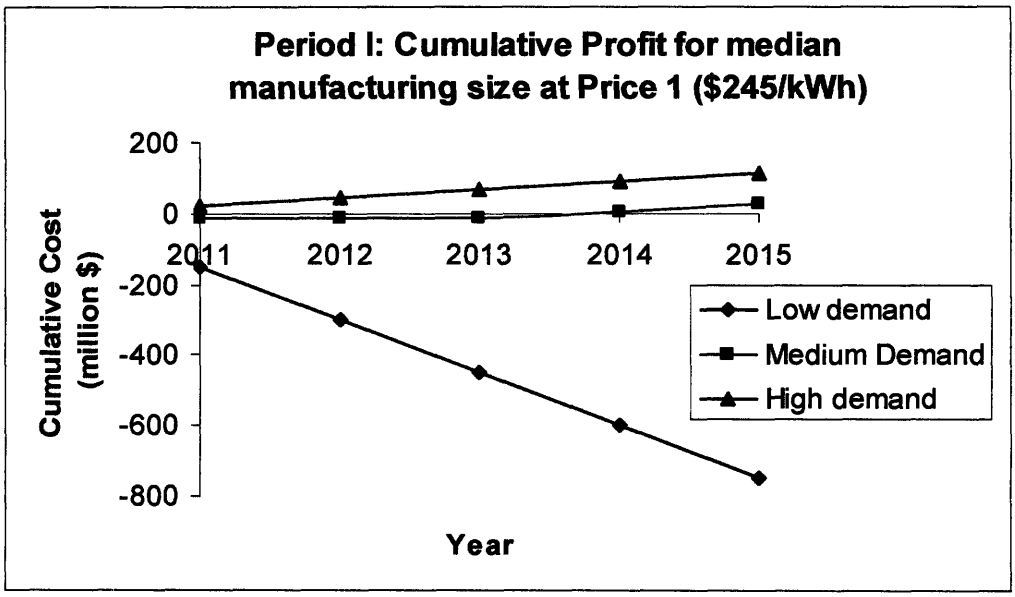

Figure 34 (b): Cumulative profit of medium manufacturing size at Price 1 for different market demands

Having a small plant size in Period I not only minimizes expected financial lost by 2015, but also provides much more flexibility in terms of plant restructuring at the beginning of Period II, when the market demand information is readily available. Table 7 reflects such high degree of flexibility at different demand scenarios. Figure 35 shows the resultant cumulative profits for each demand scenarios with the optimal pricing and manufacturing strategies chosen for Period I and II.

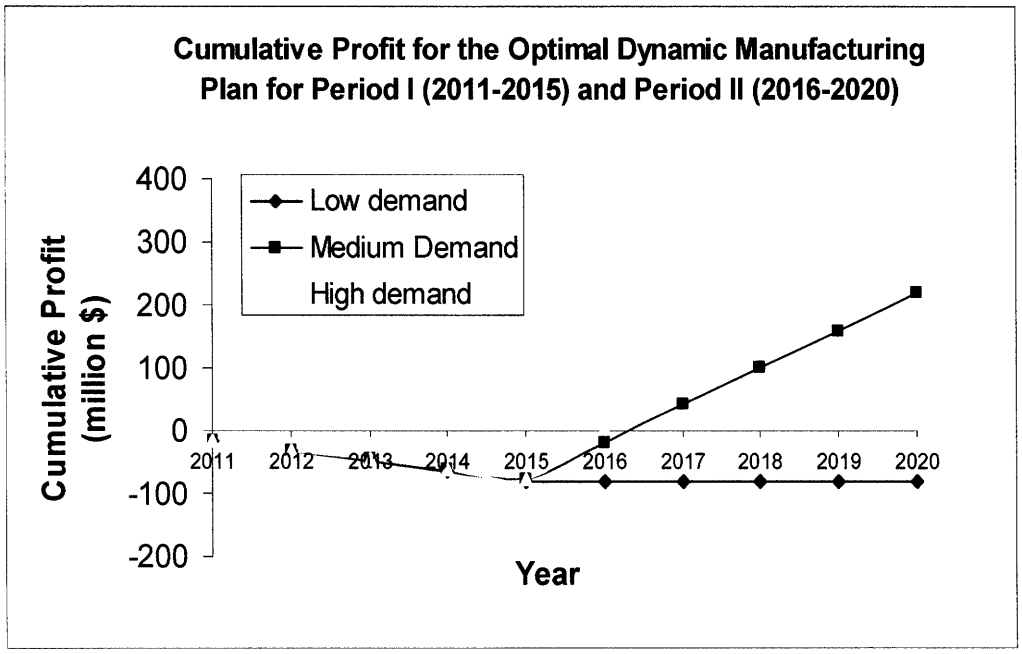

Figure 35: Cumulative profit for the optimal dynamic manufacturing plan for Period I (2011-2015) and Period II (2016-2020) for different market demands

4.5 Conclusion

As electrical energy storage device in HEVs, EESUs have relatively high multi-utility compared to the existing batteries based on the reported performance, sharpening the market competitive edge of EESUs. However, to ensure sufficient market demand in manufacturing Period I (2011-2015), a lower price ($245/kWh) is suggested in order to obtain sufficient market penetration. A small plant size is also chosen in order to mitigate the expected financial risks. In such scenario, a production cost breakdown of average specific EESU ($/kWh) is illustrated in Figure 36, in which the raw materials and utility cost contribute the largest proportion. As a result, the initial investment of an EESU plant is estimated to be $20 million.

The pricing and manufacturing strategies in the Period II (2016-2020) are reactions to the actual market demand by the end of Period I. Hence, if the market demand is found to be low, then the plant should be closed to minimize further financial loss. If, however, a medium demand is seen, then the plant is suggested to expand to the medium scale with the price increased to $270/kWh, resulting in a predicted breakeven occurring around mid-2016 and an expected NPV of $218 million for ten years of operation. In the case of high demand, a large scale plant size and the higher price ($270/kWh) should be chosen, resulting in the breakeven occurring at the end of 2015 and the expected NPV of $332 million. Considering different possibilities of the market demand and a 15% of discount rate, the weighted Net Present Value (NPV) of the proposed business is expected to be $83 million, a four-fold of return on investment in ten years.

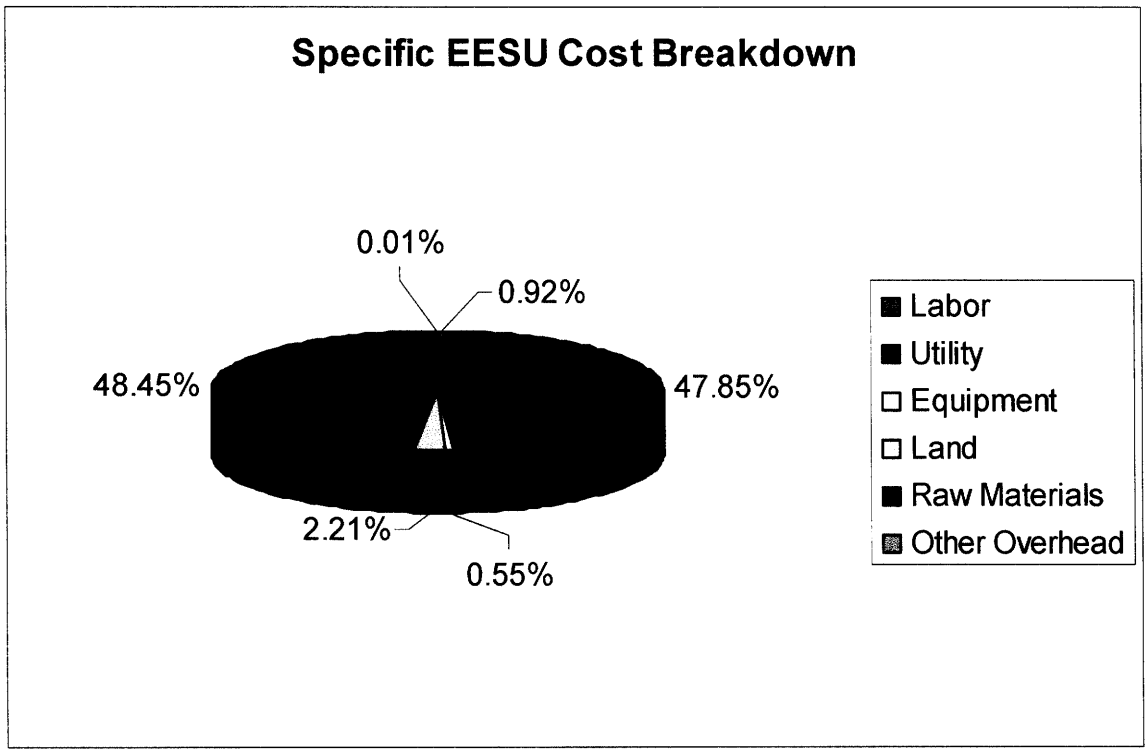

Figure 38: Specific EESU cost breakdown in the optimal pricing and plant sizing strategy

Chapter 5 Intellectual Property Overview

Released intellectual properties, especially patents, provide information about the maturity of the technologies, proposed production plans and the expected performance benchmark of the products. From the assessment of the existing patents, the strategies of establishing new intellectual properties can be inferred in order to protect a competitive commercialization plan.

5.1 EESU Patents

The most relevant descriptions of EESU are series of patents disclosed by Richard Weir, CEO of a startup company EEStor Inc., aiming to commercialize EESU in automotive industry. In US Patent 20040071944 (04/12/2001), a general introduction of EESU's structure and materials is proposed. The energy storage mechanism and a wide spectrum of applications are as well introduced.

In terms of EESU structure and materials, it claims that:

1) Single EESU unit comprises of dielectric materials and Nickel electrodes.
2) The dielectric materials comprise of basis particles of composition modified barium titanate powder, outside of which a first layer aluminum oxide and a second layer of calcium magnesium aluminosilicate glass are coated.

In terms of energy storage mechanism, it claims that:

1) The double coatings around the basis particles to form a void free body result in high breakdown strength (~5.10^6 V/cm).
2) Composition modified barium titanate powders intrinsically possess high permittivity (~33,000).

In terms of applications, it claims that EESUs can be used to

1) Power electrical vehicles
2) Act as a portable energy source for residential commercial and industrial applications
3) Power portable electronic device
4) Power remote devices

In US Patent 07033406 (04/12/2001), detailed processing methods of EESU are proposed. The following bullet points sequence the processes:

a) Preparing a wet-chemical calcined composition-modified barium titanate powder

b) Fabricating an aluminum oxide (Al_2O_3) coating with the use of aluminum nitrate nonahydrate precursor applied by wet chemical means, then calcining at 1050°C.

c) Fabricating a second coating of calcium magnesium aluminosilicate glass derived from alcohol-soluble precursors using wet chemical means followed by calcining at 500° C.

d) Blending the double-coated basic powder with a screen-printing ink

e) Screen-printing into interleaved multilayers of alternating offset nickel electrode layers and double-coated basic particles.

f) Drying and cutting the screen-printed multilayer components into a specified rectangular area;

g) Sintering the screen-printed multilayer components, hot isostatically pressing the closed-pore porous ceramic bodies with a specified pressure, into a void-free condition

i) Grinding and connecting nickel side bars

k) Heat bonding at 800°C for 20 minutes

l) Wave soldering each side of the conducting bars and assembling

More detailed ceramic powder preparation methods designed for EESU are disclosed in US Patent 20070148065 (03/07/2006), in which the wet chemical method and the precursor chemicals are described in manufacturing sequences.

5.2 Other Patents of Interest

Solid State Electrical Storage Device

US Patent 5973913 (10/26/1999): Covalent Associates, Inc., MA, received a patent on the development of nonaqueous electrical storage device based on the structure of electrochemical capacitor, comprising of high surface area electrodes, conductive polymer current collector, a separator and a thermoplastic gasket sealing. Electrode materials are selected from the group consisting of particulate carbon, carbon fiber and a doped polymer electrode which all inherently possess high surface area, and thus, potential for high specific capacitance. Electrode materials are selected from the group

consisting of $EMIPF_6$ in an alkyl carbonate solvent, tetralkylamine salts in an organic solvent, and Et_4NBF_4 in propylene carbonate.

US Patent 6078494 (06/20/2000): the concept of solid state multilayer ultracapacitor closed to the core technology of EESU was introduced by Peter Hansen of US Philips Corporation before EEStor. A dielectric ceramic composition including a doped calcium-zirconium-titanate, $(Ba_{0.09575}Nd_{.0.0025}Ca_{0.04})[Ti_{0.995}\text{-}xMn_{0.0025}Y_{0.0025}Zr_x]_zO_3$, was proposed for the dielectric material characterized by high dielectric constant. The multilayered structure was proposed with alternating nickel or nickel alloy as inner electrodes.

US Patent 6243254 (06/05/2001): the ceramic composition and the architecture of the multilayer ceramic ultracapacitor were closely observed by Murata Manufacturing Co., Ltd., Japan. The basic dielectric materials composition was identified as $(Ba_{1\text{-}x}Ca_xO)_m$ $TiO_2 + \alpha Re_2O_3 + \beta MgO + \gamma MnO$ with the particle size of 0.1 to 0.7 microns. Structurally, a plurality of dielectric layers of Ni or Ni alloy is proposed as inner electrodes; external electrodes consist of sintered layer of conductive metal powders or glass frit in electrical continuity to a plurality of inner layers and being on the surface of ultracapacitor.

US Patent 6268054 (07/31/2001): Cabot Corporation, MA, received a 73-claim patent on the close processing control of dispersing barium titanate powders, which will affect material high breakdown voltage to a substantial extent. The patent proposes that higher breakdown voltage can be achieved using thin, fine grained powders by high shear mixing.

Method of Solid State Ultracapacitor Components Packaging

US Patent 5711988 (01/27/1998), 5867363 (02/02/1999) and 5800857 (09/01/1998) 6005764 (12/21/1999): Pinnacle Research Institute, CA, received patents on process improvement of structure integration for electrical charge storage device. The innovations include

• Producing an array of substantially uniform microprotrusions as charge storage device separator by creating porous metal oxide on the conducting electrodes with polymer protrusion into the porosities.

• Producing a dry preunit in a condition to have the electrode surfaces contacted with a ion permeable or semipermeable non-aqueous or aqueous electrolyte mainly by depositing uniform insulating microprotrusions

• Producing a sealable and electrically insulating band of organic polymer on the perimeter edges of an individual electrode to eliminate leakage current.

Battery and Ultracapacitor Hybrid Energy Storage System

US Patent 5738919 (04/14/1998): Motorola, Inc., IL, received a patent on the architecture and power control methods of a hybrid electrical energy source consisting of two energy storage devices, one of which is designed to provide a constant current output and the other to provide intermittent energy bursts. In addition, the system also consists of a current controller disposed between the two devices. Coupled with two switches, the current controller is responsive to current pulses to avoid current interference between the two devices. This technology can be used to simulate the energy utilization in the HEV powertrain system.

US Patent 5744258 (04/28/1998) and US Patent 5797971 (08/25/1998) are another two patents received by Motorola Inc., IL, on a high power, high energy hybrid electrode designed to allow co-deposition of two different electroactive materials demonstrating high rate capability and high energy density capability respectively. The electrode comprises of an anode with the first electroactive material selected from group consisting of cadmium, metal hydrides, lead, and zinc, and a cathode the first electroactive material is selected from the group consisting of nickel oxide, lead oxide, and silver. The second electroactive material is deposited on both sides of the electrode from the group consisting of Nb, Hf Ti, Ta, Li, Fe, Zn, Sn, Ru, Ag, Pt, Ir, Pb, Mo, W, Ni, Co and their oxides, hydroxides, hydrides, carbides, nitride or sulfites, and carbon, etc. The materials are engineered to possess high specific capacitance and electronic conductivity which typically include $RuO_2.xH_2$ O powder and carbon black or carbon fiber. These innovations facilitate the EESU system to possess both stable current with high energy density and required high power density with high current pulses.

5.3 Conclusion

The most relevant intellectual properties to the manufacture of EESUs are series of Weir's patents issued to EEStor Inc. around 2006 which detail the materials selection, manufacturing process and performance prediction. However, Weir's patents are regarded relatively weak in terms of freedom to operate and exclusive development with the major limitations including:

(a) The Infringement of existing Intellectual Property

The Intellectual Property infringement would eliminate the freedom to operate the issued patents. Weir's claim of using barium titanate powder as the base material for the dielectric electrolyte infringes with US Patent 6078494 (06/20/2000); the claims on dielectric structure of multi-layered electrode and electrolyte imfringes with US Patent 6243254 (06/05/2001). Other areas of infringement may include the production of barium titanate powders and packaging methods.

(b) Narrow Claims

The claims of Weir's patents are narrowly and specifically expressed, which would not effectively exclude competitive developments in EESU manufacturing and integration. For instance, minor changes in the base ceramic composition, such as in the US Patent 6243254 (06/05/2001), would not be regarded as IP infringement since the composition in Weir's Patent 20040071944 (04/12/2001) is too specifically defined.

Hence, there is still substantial room for developing the intellectual proprietary rights in the competitive commercialization of EESUs. The critical areas requiring IP protections include powder production and manufacturing, heat treatment process optimization and final component packaging. Broader claims are suggested as a patent strategy in order to maximize freedom to operate and ensure exclusive technology development.

Chapter 6 Conclusion

This report assesses Solid State Ultracapacitors (SSUs) from the technology and market perspectives. The technological uniqueness of SSUs is identified as high voltage DC operation to obtain high energy density. Two concepts of SSUs, namely Electrical Energy Storage Unit (EESU) and Organic Solid State Ultracapacitor (OSSU) are compared technologically. Both models seek the enhancements in DC permittivity and dielectric breakdown voltage through the selection and engineering of electrolyte materials. With composition modified barium titanate electrolyte, EESU is recognized as the most successful model in terms of energy density achievement. With conductive particle filled polymer electrolyte, OSSU is not regarded as a competitive SSU model since no energy density enhancement has been observed from experiments or modeling, which may be due to the absence of giant permittivity under DC and the futility of conductive phase dispersion with no contribution to the energy storage capability. Performance comparisons between EESU PHEVs and battery PHEVs are carried out based on the projected PHEV performance and reported EESU properties. It is concluded that EESU PHEVs may excel battery PHEVs both in terms of manufacturing cost and fuel efficiency although appreciable technology and financial uncertainties exist. A dynamic startup EESU manufacturing plan is conducted to maximize the expected Net Present Value and minimize financial risks from 2011 to 2020. Considering the unpredictabilities in market demand, the optimized manufacturing plan requires the initial investment of $20 million to obtain four-fold of the expected return. In terms of Intellectual Property strategy for a competitive EESU development plan, room for the establishment of IP proprietary rights exists if innovations can be protected by broader claims in key technological areas.

References

1. Aowei 2007: Ultracapacitor Electric Passenger Bus, Ultracapacitor Tourist Car, 2007, Shanghai Aowei Technology, available on-line at http://www.aowei.com/english/case.htm

2. Bard, Allen and Faulkner, Larry, 2001: Electrochemical Methods Fundamentals and Application, 2nd ed., 2001, John Wiley & Sons

4. Barsoukov E., Macdonald R. J. 2005: Impedance Spectroscopy: Theory, Experimental, and Applications, 2nd Ed, 2005, John Siley & Sons, New Jersey

5. Böttcher C.J.F. 2001, Theory of Electric Polarization: Dielectric Polarization, , ISBN 0-44441-579-3

6. Department of Energy (DOE), Office of Science, 2007, Technology and Applied R&D Needs for Electrical Energy Storage, Contributors: G. Gruzalski et al.

7. Gonder, Markel, Simpson and Thornton, 2006: Using GPS Travel Data to Assess the Real World Driving Energy Use of Plug-in Hybrid Electric Vehicles (PHEVs), TRB 86th Annual Meeting, Washington, D.C., 2007

8. Hansen 2000, US Patent 6,078,494, Multilayer Capacitor Comprising barium-titanate coped with silver and rare earth metal, US Philips Corporation

9. Helmholtz, H. von, Ann. Phys. (Leipzig), vol. 89, p. 211 (1853).

10. Isomil, 2006, Isolation Materials and Dielectric Strength, available on-line at http://www.isomil.de/english.htm?/cont/en/insulation_materials.htm

11. Kuwata et al. 1985, Electrical Properties of Perovskite-Type Oxide Thin-Films Prepared by RF Sputtering, Jpn. J. Appl. Phys., Part 1, 1985, 24, 413-15

12. Linden D and Reddy T.B. 2001, Handbook of Batteries, 3rd Ed., McGraw-Hill Companies, Inc., New York, 2003

13. Markel, T. and Simpson, A. "Energy Storage Considerations for Grid-Charged Hybrid Electric Vehicles." *IEEE Vehicular Technologies Conference.* September 7-9, 2005. Chicago, IL.

14. Pecharroman C. and Moya J.S. 2000, Experimental evidence of a giant capacitance in insulator–conductor composites at the percolation threshold, *Adv. Mater.* **12** (2000) (4), pp. 294–297.

15. Pillot, C., 2005 (Avicenne) from the 23rd International Battery Seminar & Exhibit, March 13-16, Ft. Lauderdale, FL.

16. Rosenkranz, C. "Deep Cycle Batteries for Plug-in Hybrid Application" Presented at *EVS-20 Plug-in Hybrid Workshop*. Nov. 15, 2003.

17. Roth, R., F. Field and J. Clark; "Materials selection and multi-attribute utility analysis;" *Journal of Computer-Aided Materials Design*; V 1 No 3; ESCOM Science Publishers, Leiden, The Netherlands; October, 1994.

18. Saito T., Takemoto S., and Iriyama T., 2005: Resistivity and Core Size Dependencies of Eddy Current Loss for Fe–Si Compressed Cores, IEEE TRANSACTIONS ON MAGNETICS, VOL. 41, NO. 10

19. Search 2007, Encyclopedia: Permittivity, available on-line at http://www.search.com/reference/Permittivity

20. U.S. Department of Transportation 2004, Federal Highway Administration "Highway Statistics 2004." Available on line at http://www.fhwa.dot.gov/policy/ohim/hs04/index.htm

21. U.S. Energy Information Administration 2006, Average Retail Price of Electricity to Ultimate Customers by End-Use Sector, online, www.eia.doe.gov, accessed July 16, 2007.

22. USGS 2007: US. Geological Survey, Mineral Resources Program, available on-line at http://minerals.usgs.gov/, accessed on July 20th, 2007

23. Valant M., Dakskobler A., Ambrozic M. and Kosmac T. 2006, Giant permittivity phenomena in layered $BaTiO_3$–Ni composites, Journal of European Ceramic Society, Volume 26, Issue 6, 2006, Pages 891-896

24. Weir R.D. and Nelson C.W. 2001, Electrical-Energy-Storage Unit (EESU) Utlizing Cermaic and Integrated-Circuit Technologies for Replacement of Electrochemical Batteries, Eestor, Inc, 2001, US Patent 7,033,406

25. Wikipedia 2007: Toyota Prius, available on-line at http://en.wikipedia.org/wiki/Toyota_Prius

26. Zurek 2007, Ragone Plot, Maxwell Technologies, available on-line at http://www.maxwell.com/ultracapacitors/index.html or http://en.wikipedia.org/wiki/Image:Supercapacitors_chart.svg, accessed 07/22/2007

Appendix 1: Terminologies in HEV and PHEV

A PHEV is a hybrid-electric vehicle (HEV) with the ability to recharge its electrochemical energy storage with electricity from an off-board source (such as the electric utility grid).

All-Electric Range (AER) – defined as the distance in miles that a fully charged PHEV can drive on stored electricity before needing to operate its engine. According to this definition, a PHEV20 can drive 20 all-electric miles (32 kilometers) on the test cycle before the first engine turn-on.

Charge-sustaining (CS) mode – An operating mode in which the state-of-charge of the energy storage system over a driving profile may increase and decrease but will by the end of the cycle return to a state with equivalent energy as at the beginning of the period.

Charge-depleting (CD) mode – An operating mode in which the state-of-charge of the energy storage system over a driving profile will have a net decrease in stored energy

Degree of hybridization (DOH) – defined as the ratio of motor power to total motor plus engine power

Electrified miles – Is the sum of all miles driven with the engine off including those after the engine first turns on.

PHEVxx – A plug-in hybrid vehicle with sufficient energy to drive xx miles electrically on a defined driving profile usually assumed to be urban driving.

***SOC*– State-of-charge** of the energy storage system: The fraction of total energy capacity remaining in the battery.

Utility factor– A measure of the fraction of total daily miles that are less than or equal to a specified distance based on typical daily driving behavior.

Appendix 2: Cost Model of EESU Manufacturing

Assuming annual production volume of 12,500,000 lb

MAJOR MATERIAL INPUT			Weighted Cost
Barium Titanate Powder	13.63636364	/lb	13.16288
Nickel	14.54545455	/lb	
Balance (Nd, Mg, Ca, surfactant, etc)	5	/lb	
EXOGENOUS DATA			
Annual Production Volume	12,500,000	(lbs/yr)	
Facility Production Capacity	12,500,000	(lbs/yr)	
Product Life	5	yrs	
Working Days/Yr	350		
Downtimes			
No Operations	2	hrs/day	
Planned Paid	1	hrs/day	
Planned Unpaid	1.2	hrs/day	
Capital Recovery Rate	0.1		
Scrap Rate	0.1		
Accounting Life of Machine	20	yrs	
Overhead Burden (% fc)	0.35		
PROCESS CALCULATIONS			
Day Production Volume	35714.28571	lbs/day	
Hour Production Volume	1803.751804	lbs/hr	

EQUIPMENT					
	Lbs Produced		Price	Lbs Processed	
Wet-chemical and Calcine	200	/hr	50000	2400.793651	/hr
Screen Printing	200	/hr	100000	2182.539683	/hr
Annealing Furnace	200	/hr	50000	1984.126984	/hr
Grinding	200	/hr	50000	1803.751804	/hr

COST ANALYSIS			
Items	Units Required/lb		Costs/lb
Cacine and Wet		1	worker/machine
Materials	1.331	lbs	17.51979167
Electricity	13.47192	kWH	0.9430344
Labour	0.005544	manhours	0.08316
Screen Printing		1	worker/machine
Electricity	5.544	kWH	0.38808
Labour	0.005544	manhours	0.08316
Argon Gas		L	0
Hydrogen Gas		L	0
Printer Head	4.5351E-05	/lb	0.004535147
Annealing		1	worker/machine
Electricity	12.1968	kWH	0.853776
Labour	0.005544	manhours	0.08316
Grinding		1	worker/sieve
Electricity	1.1088	kWH	15.12
Labour	0.005544	manhours	0.08316
VAR COSTS/lb			35.16185721
Fixed Costs			
Land			10000000
Equipment			2500000
TOTAL FIXED COST			12500000
Fixed Costs/lb			1
TOTAL COSTS/lb			36.16185721

Appendix 3: Unit cost of EESU at Different Levels of Capacity Utilization

Plant Capacity Assumed 45,000 units to 450,000 units

	Plant Capacity (Unit of EESU)	**450000**	**360000**	**225000**	**180000**	**45000**
Production Volume (Unit of EESU)						
45000		1040.23	856.3218	580.4598	481.0345	209.7701
90000		568.9655	477.0115	339.0805	227.5862	
135000		413.7931	350.5747	258.6207	195.4023	
180000		333.3333	287.3563	221.2644		
225000		287.3563	251.1494	197.1264		
270000		258.6207	226.4368			
315000		235.6322	208.6207			
360000		218.3908	195.4023			
405000		205.1724				
450000		194.8276				

Appendix 4: Utility Function of EESU

Single Untility Function – EESU Cost

Cost ($/kWh)	U(Cost)
150	1
180	0.9
210	0.8
240	0.7
270	0.4
300	0.3
330	0.15
360	0.05
390	0

Single Utility Function – AER

AER (miles)	U (AER)
0	0
20	0.25
40	0.45
60	0.6
80	0.7
100	0.76
120	0.81
140	0.84
160	0.9
300	1

Multi-utility Function of EESU

Cost AER	0	20	40	60	80	100	120	140	160	300	K
150	0.7	0.625	0.725	0.8	0.85	0.88	0.905	0.92	0.95	1	-0.57143
180	0.45	0.58	0.684	0.762	0.814	0.8452	0.8712	0.8868	0.918	0.97	
210	0.4	0.535	0.643	0.724	0.778	0.8104	0.8374	0.8536	0.886	0.94	
240	0.35	0.49	0.602	0.686	0.742	0.7756	0.8036	0.8204	0.854	0.91	
270	0.2	0.355	0.479	0.572	0.634	0.6712	0.7022	0.7208	0.758	0.82	
300	0.15	0.31	0.438	0.534	0.598	0.6364	0.6684	0.6876	0.726	0.79	
330	0.075	0.2425	0.3765	0.477	0.544	0.5842	0.6177	0.6378	0.678	0.745	
360	0.025	0.1975	0.3355	0.439	0.508	0.5494	0.5839	0.6046	0.646	0.715	
390	0	0.175	0.315	0.42	0.49	0.532	0.567	0.588	0.63	0.5	